People's Democratic Republic of Algeria

Ministry of Higher Education and Scientific Research

Echahid Hamma Lakhdar University of El-Oued

Faculty of Technology

Department of Electrical Engineering

MASTER'S THESIS

Presented in Partial Fulfillment of the Requirements for the Degree of

ACADEMIC MASTER

Domain: Science and Technologie

Field: Electrotechnics

Specialty: Electrical Machines

Presented by: **Djaafri Abdelaali**

Thesis Title

Design and Implementation of an IoT-Based Smart Water Pumping System for Automated Irrigation Control and Real-Time Monitoring

Board of Examiners:

Dr. Ben Gharbi Abdelkader	**President**	University of El-Oued
Dr. Maamir Mediha	**Examiner**	University of El-Oued
Dr. Cherif Hakima	**Supervisor**	University of El-Oued
Dr. Allag Nassiba	Co-**Supervisor**	University of El-Oued

Academic year: 2025/2026

Abstract

The Internet of Things (IoT) is experiencing increasing adoption in several sectors, including industry, healthcare, and especially agriculture. This technology offers innovative and revolutionary solutions for monitoring and controlling systems, thanks to its ease of deployment, low cost, and ability to ensure long-distance communication.

In agriculture, the IoT plays a crucial role in optimizing pumping systems and water resource management. In this context, this work proposes the design and implementation of an intelligent, real-time monitoring and control system for an agricultural pumping system, based on an IoT architecture.

The system is based on a TMS320F28379D microcontroller, which acts as the main control unit. This microcontroller acquires and processes data from voltage and current sensors to analyze operating conditions and detect electrical anomalies. The collected information is then transmitted to an ESP32 module via UART communication. The ESP32 transmits data to a second ESP32 module using LoRa technology, ensuring long-range wireless communication. This second module connects to a Wi-Fi network, enabling data to be sent to a server and displayed on a dedicated mobile application The mobile application offers an intuitive interface for real-time monitoring of electrical parameters, displaying system status, and remotely controlling the pump.

The system also incorporates advanced protection for a three-phase asynchronous motor against electrical faults such as overvoltage, undervoltage, overload, phase loss, imbalance, and reverse rotation. Experimental results confirm the system's performance in terms of reliability, protection, and monitoring, making it suitable for agricultural applications, particularly in remote or resource-limited areas.

Keywords: Current Sensors, ESP32, IoT, Mobile Application, LoRa, Three-phase motor protection, TMS320F28379D, UART, voltage.

ملخص:

يشهد إنترنت الأشياء (IoT) انتشارًا متزايدًا في قطاعات عديدة، تشمل الصناعة والرعاية الصحية، وخاصة الزراعة. توفر هذه التقنية حلولًا مبتكرة وثورية لأنظمة المراقبة والتحكم، بفضل سهولة نشرها وانخفاض تكلفتها وقدرتها على ضمان الاتصال عن بُعد.

في القطاع الزراعي، يلعب إنترنت الأشياء دورًا محوريًا في تحسين أنظمة الضخ وإدارة موارد المياه. في هذا السياق، يقترح هذا العمل تصميم وتنفيذ نظام ذكي للمراقبة والتحكم في الوقت الفعلي لنظام ضخ زراعي، قائم على بنية إنترنت الأشياء. يعتمد النظام على وحدة تحكم دقيقةTMS320F28379D ، والتي تعمل كوحدة تحكم رئيسية.

تقوم هذه الوحدة باستقبال ومعالجة البيانات من مستشعرات الجهد والتيار لتحليل ظروف التشغيل والكشف عن أي خلل كهربائي. ثم تُرسل المعلومات المُجمعة إلى وحدة ESP32 عبر منفذ UART تقوم وحدة ESP32 بدورها بإرسال البيانات إلى وحدة ESP32 أخرى باستخدام تقنيةLoRa ، مما يضمن اتصالًا لاسلكيًا بعيد المدى.

تتصل هذه الوحدة الثانية بشبكة واي فاي، مما يتيح إرسال البيانات إلى خادم وعرضها على تطبيق جوال مخصص. يوفر التطبيق واجهة سهلة الاستخدام لمراقبة المعايير الكهربائية في الوقت الفعلي، وعرض حالة النظام، والتحكم عن بُعد في المضخة. كما يتضمن النظام حماية متقدمة لمحرك ثلاثي الأطوار غير متزامن ضد الأعطال الكهربائية مثل الجهد الزائد، والجهد المنخفض، والحمل الزائد، وفقدان الطور، وعدم التوازن، والدوران العكسي. تؤكد النتائج التجريبية أداء النظام من حيث الموثوقية والحماية والمراقبة، مما يجعله مناسبًا للتطبيقات الزراعية، لا سيما في المناطق النائية أو ذات الموارد المحدودة.

الكلمات المفتاحية: مستشعرات التيار، ESP32، إنترنت الأشياء، تطبيق جوال، LoRa، حماية محرك ثلاثي الأطوار، TMS320F28379D، UART، الجهد.

ACKNOWLEDGEMENTS

In the name of Allah, the Most Gracious, the Most Merciful, I express my deepest gratitude for granting me the strength, perseverance, and determination necessary to complete this work.

I would like to extend my sincere appreciation to my supervisor, **Dr. Hakima Cherif**, and my co-supervisor, **Dr. Allag Nassiba**, for their invaluable guidance, insightful advice, and continuous support throughout the preparation of this dissertation. Their expertise, academic rigor, and constructive feedback have been instrumental in shaping this research and bringing it to completion. I am deeply grateful for the time, patience, encouragement, and dedication they devoted to supervising this work. Their support and commitment have greatly contributed to the successful completion of this thesis.

My heartfelt thanks are also addressed to the members of the examination committee for accepting to evaluate this dissertation. I highly appreciate the time and effort they have invested in reviewing this work, as well as their valuable observations, comments, and recommendations, which have contributed to improving its quality.

I would like to express my sincere gratitude to **Dr. Chouaib Labiod, Dr. Nabil Aouragh, Mr. Dia Zakaria, Ms. Marwa Youmbie**, all the members of the **LEERE Laboratory**, and the **Institute Vision Expertise Formation (IVEF)** for their assistance, encouragement, and the stimulating scientific environment they provided throughout the realization of this project. Their support, collaboration, and commitment to academic and professional development have greatly enriched this research experience.

I am equally indebted to all the professors and teachers who have contributed to my academic education and professional development over the years. Their dedication to teaching, commitment to excellence, and passion for knowledge have played a fundamental role in shaping my academic journey.

Dedication

I would like to express my profound gratitude to my beloved mother for their unconditional love and unwavering support.

Special thanks go to my wife **Dr. KADDOURI SOUAD**, whose encouragement, understanding, and sacrifices have been a constant source of motivation. I am equally grateful to my daughters, ***Celine*** and ***Alaa***, whose love and joy have inspired me throughout this challenging yet rewarding journey.

Finally, I extend my sincere thanks to all those who have contributed, directly or indirectly, to the successful completion of this dissertation. Their support, encouragement, and confidence in my abilities are deeply appreciated.

To all of them, I offer my deepest respect and gratitude.

TABLE OF CONTENTS

TABLE OF FIGURE

General Introduction

General Introduction

Agriculture is one of the fundamental pillars of the global economy and food security. It plays a crucial role in supporting national development by ensuring the production of food resources required to meet the needs of a growing population. Among the various factors influencing agricultural productivity, irrigation management remains one of the most critical, as it directly affects crop yield, water consumption, and the sustainability of farming activities.

The importance of efficient irrigation is particularly evident in remote and geographically challenging regions, where limited water resources, irregular rainfall patterns, and inadequate infrastructure often hinder agricultural development. In such environments, ensuring reliable water supply and optimizing water utilization have become major challenges. Consequently, the adoption of advanced technologies for intelligent water management is increasingly recognized as an essential requirement for achieving sustainable agricultural production.

In recent years, the rapid advancement of the Internet of Things (IoT), embedded systems, and wireless communication technologies has opened new opportunities for the development of smart irrigation systems. Numerous research efforts have focused on designing intelligent monitoring and control platforms capable of collecting real-time data, automating irrigation processes, and improving the overall efficiency of water resource management. These studies have proposed various architectures based on sensors, microcontrollers, cloud services, and mobile applications, providing farmers with effective tools for remote supervision and decision-making.[1]

Despite the significant progress achieved in this field, several limitations remain. Most existing solutions rely on conventional microcontrollers with limited processing capabilities and depend heavily on communication infrastructures such as Wi-Fi or cellular networks, which may not be available in isolated rural areas. Furthermore, many systems focus primarily on irrigation automation while providing limited functionality for advanced monitoring, fault diagnosis, and equipment protection.

To address these limitations, this thesis proposes the design and implementation of an IoT-based smart water pumping system for automated irrigation control and real-time monitoring. The proposed architecture combines the high-performance TMS320F28379D microcontroller with ESP32 modules and LoRa communication technology. The TMS320F28379D is employed as the main processing unit due to its superior real-time computational capabilities, enabling advanced signal processing, monitoring, and protection functions. LoRa technology is integrated to ensure reliable long-range communication, making the system particularly suitable for remote agricultural environments where conventional communication networks are unavailable or unreliable.

In addition, the proposed system incorporates an intelligent monitoring and protection strategy for three-phase pump motors. The developed solution is capable of detecting and managing several electrical faults and abnormal operating conditions, including overvoltage, undervoltage, overload, phase loss, phase reversal, voltage unbalance, and dry-running conditions. By integrating monitoring, control, communication, and protection functions within a unified architecture, the system reduces dependence on conventional protection devices while enhancing operational reliability and system autonomy.

The main objective of this work is therefore to develop a reliable, intelligent, and cost-effective irrigation management platform capable of improving water resource utilization, ensuring safe operation of pumping equipment, and providing real-time monitoring and remote control functionalities. The proposed solution contributes to the advancement of smart agriculture technologies and offers a practical approach for supporting sustainable agricultural development, particularly in remote and resource-constrained regions.

This dissertation is organized as follows. Chapter 1 presents a comprehensive literature review of IoT-based smart irrigation systems and real-time monitoring technologies. Chapter 2 discusses the main electrical faults affecting pump motors and the associated protection techniques, including MATLAB/Simulink modeling and analysis. Chapter 3 describes the design, implementation, and experimental validation of the proposed system, followed by the presentation and discussion of the obtained results. Finally, the dissertation concludes with a summary of the main contributions and recommendations for future research.

Chapter 1

Literature Review of Smart Irrigation Systems and IoT Technology

1.1 Introduction

The growing demand for food production, increasing water scarcity, and the impacts of climate change have become major challenges for modern agriculture. Since irrigation accounts for a significant portion of global freshwater consumption, improving water management has become essential for ensuring agricultural productivity and sustainability [1].

In recent years, the Internet of Things (IoT) has emerged as a promising technology for smart irrigation applications. By integrating environmental sensors, embedded controllers, and wireless communication networks, IoT-based systems enable real-time monitoring of agricultural conditions and automated irrigation control, leading to more efficient use of water resources [2][3]. The development of low-cost microcontrollers, such as the ESP32, together with communication technologies including Wi-Fi and LoRaWAN, has facilitated the deployment of reliable and scalable smart irrigation solutions [4].

Moreover, recent advances in Artificial Intelligence (AI), Machine Learning (ML), and Tiny Machine Learning (TinyML) have enhanced the capabilities of smart irrigation systems. These technologies allow the analysis of environmental data, prediction of crop water requirements, and optimization of irrigation strategies, thereby reducing water waste and improving agricultural efficiency [5][7]. As a result, modern smart irrigation platforms increasingly combine IoT, intelligent algorithms, and cloud or edge computing technologies to support precision agriculture and sustainable farming practices [3][8].

This chapter presents a literature review of recent IoT-based smart irrigation systems. It discusses the fundamental concepts of IoT monitoring and control, reviews the architectures and technologies used in smart irrigation applications, and examines the integration of AI and TinyML techniques. Finally, the chapter highlights current trends, challenges, and future research directions in this rapidly evolving field.

1.2. IoT-Based Monitoring and Control Systems

The Internet of Things (IoT) refers to a technological paradigm in which physical objects equipped with sensors, actuators, processing capabilities, and communication are interconnected to collect, transmit, and utilize real-time data [9]. IoT relies on several functional layers, including data perception, communication through wired or wireless networks, and information processing and analysis at the cloud or edge computing level [10].

This technology enables process automation, remote monitoring, and optimized decision-making in various fields such as smart agriculture, Industry, connected healthcare, and smart cities [9][10].

Thanks to its ability to bridge the physical and digital worlds, the IoT has become a fundamental element of digital transformation and the development of modern intelligent systems [11].

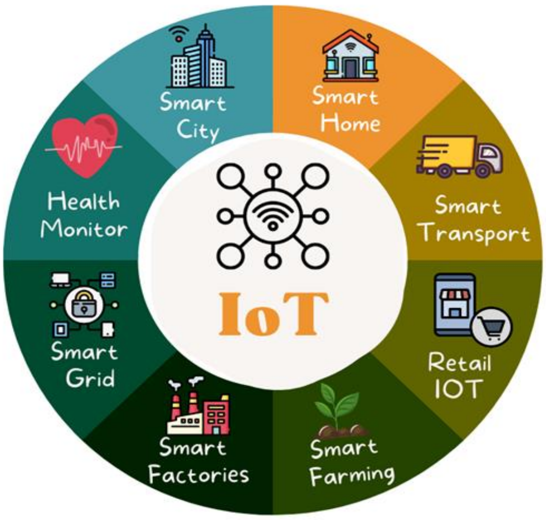

Figure 1.1: IoT Applications

1.3 Literature review of IoT-based smart irrigation systems

1.3.1 Fundamental Concepts of Smart Irrigation and the IoT

Smart irrigation is one of the most important applications of the Internet of Things (IoT) in agriculture. Its main objective is to optimize water resource use by providing crops with the necessary amount of water at the right time. Unlike conventional irrigation methods, smart systems use sensors, communication devices, and data processing platforms to monitor environmental parameters in real time and make automated irrigation decisions [12][13]. This approach helps improve agricultural productivity while reducing water losses and operating costs [14]. Recent studies show that integrating the IoT into agriculture allows for continuous monitoring of soil moisture, weather conditions, and crop status. The collected data is used to automatically trigger irrigation when certain thresholds are reached, thus improving the efficiency of water management [15][16]. These systems fall within the framework of precision agriculture, the objective of which is to maximize yields while minimizing the use of natural resources [17].

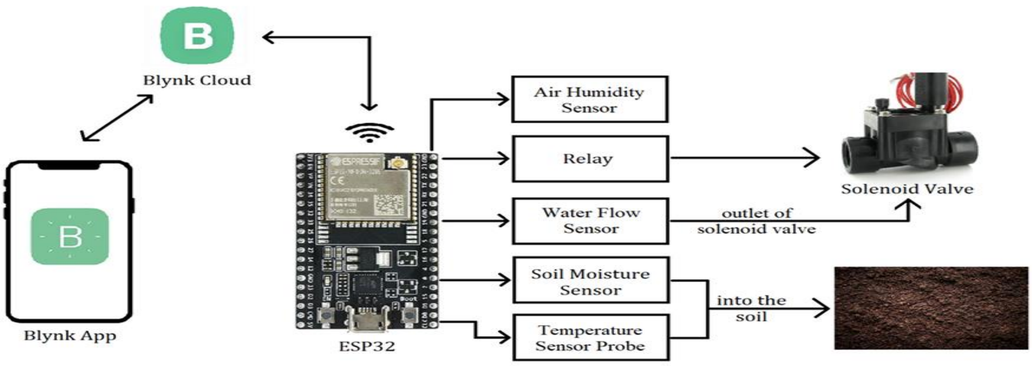

Figure 1.2: Overview of the IoT-enabled smart drip irrigation system [12].

1.3.2 IoT Architectures Used in Smart Irrigation Systems

1.3.2.1 Sensors and Embedded Devices

The studies analyzed primarily use soil moisture, temperature, and relative humidity sensors to assess crop water requirements. Pereira et al. [12] developed a smart drip irrigation system based on environmental sensors connected to an ESP32 microcontroller. Similarly, the study conducted on smart greenhouses [16] combines climate monitoring and soil moisture measurement to improve the accuracy of irrigation decisions.

The use of multiple types of sensors allows for a better understanding of agricultural conditions and improves the reliability of automated systems. Some studies also integrate light sensors and additional climatic parameters to increase the accuracy of the analyses [13][18].

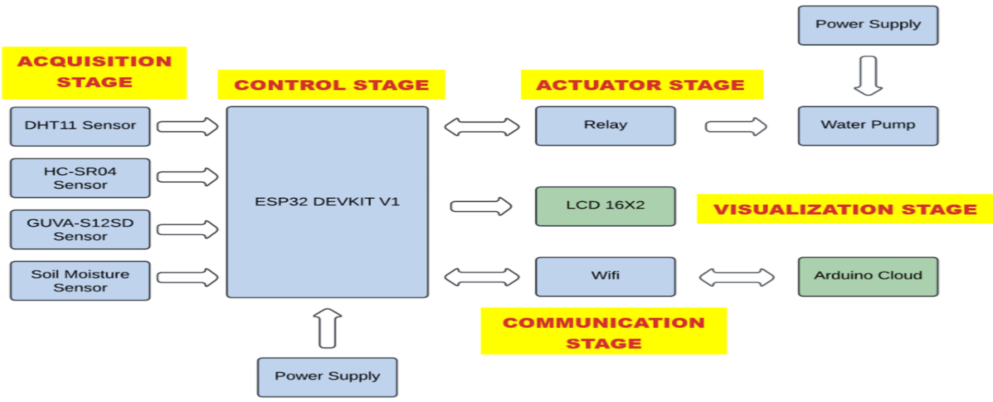

Figure 1.3: The architecture of the project in a block diagram [16].

1.3.2.2 Microcontrollers and Hardware Platforms

Analysis of studies reveals the predominance of the ESP32 microcontroller due to its low cost, low power consumption, and integrated Wi-Fi connectivity [12],[16][19]. The system proposed by Pereira et al. [12] demonstrates that the ESP32 is a cost-effective solution for small farms. Similarly, integrating the ESP32 with the Blynk platform facilitates remote monitoring and control of irrigation operations [19].

Embedded platforms enable local data acquisition and the execution of control tasks without requiring complex infrastructure. This characteristic promotes their adoption in rural areas where technological resources are limited [14].

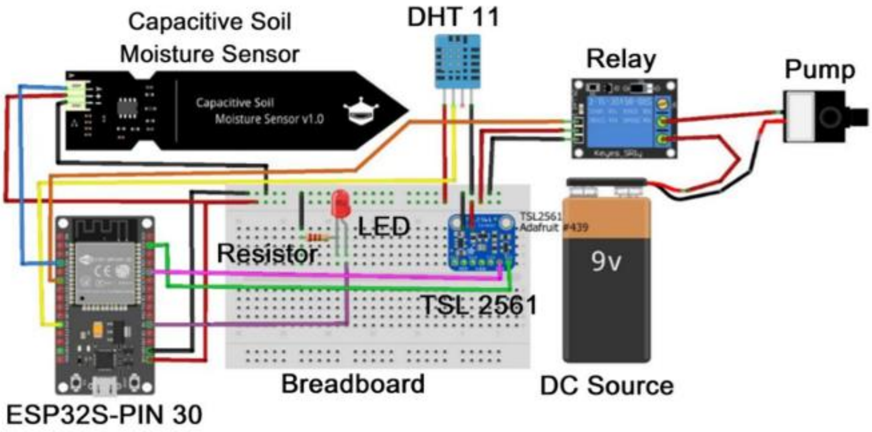

Figure 1.4: Schematic diagram of the system [14].

1.3.2.3 Communication Protocols and Cloud Platforms

The systems studied primarily use Wi-Fi to transmit data to cloud platforms. The Ubidots server enables the storage, visualization, and analysis of agricultural data in real time [17]. Another approach relies on Server-Sent Events (SSE) technologies, which ensure continuous transmission of information between IoT devices and user interfaces [13].

Cloud platforms offer significant data processing and storage capabilities, thus facilitating remote monitoring and decision-making based on the analysis of historical data [17]. However, their reliance on a stable internet connection can be a limitation in some remote agricultural areas.

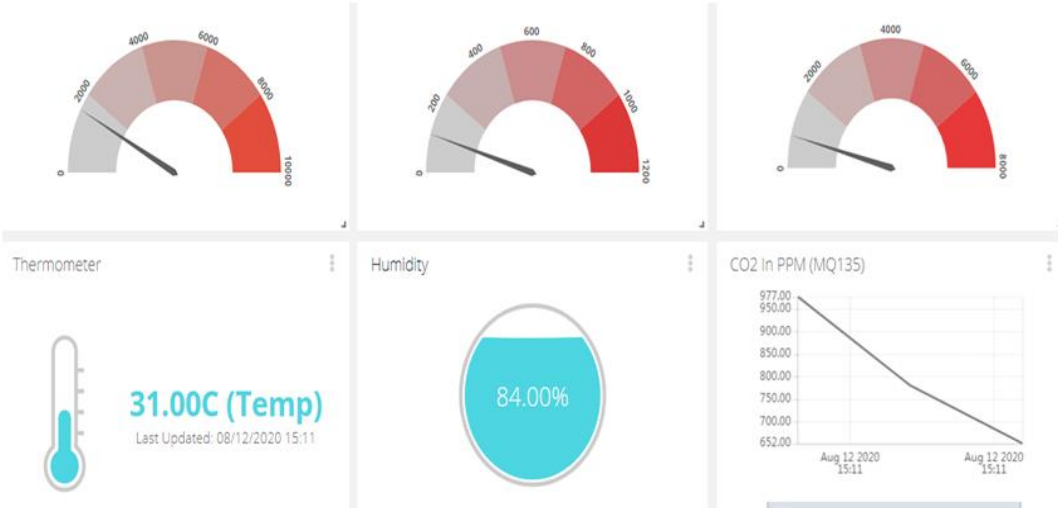

Figure 1.5: Server visualization of the proposed system [17].

1.3.3. Integration of Artificial Intelligence in Smart Irrigation

Artificial intelligence has become a central element in modern smart irrigation systems. Machine learning techniques make it possible to predict crop water requirements based on data collected by environmental sensors [20]. Kunt [20] developed an autonomous system combining IoT and artificial intelligence to automatically adjust irrigation strategies according to observed conditions.

The use of artificial intelligence not only improves the accuracy of decisions but also reduces water consumption while maintaining optimal agricultural production levels. Predictive models analyze climate trends, soil characteristics, and specific crop needs to optimize water inputs [20].

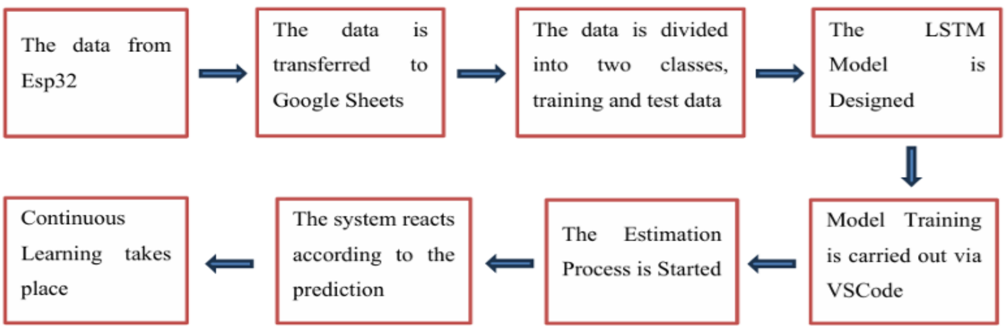

Figure 1.6: Scheme of the data management process [20].

1.3.3.1 Fuzzy Logic-Based Approaches

Among the artificial intelligence techniques identified in the literature, fuzzy logic plays a significant role. The system proposed in the study “Fuzzy-Adaptive Smart Irrigation Based on IoT” uses a fuzzy controller to automatically adapt irrigation decisions to environmental variations [18]. This approach is particularly well-suited to agricultural environments where parameters are often uncertain or difficult to model precisely.

The results show that fuzzy controllers enable more flexible irrigation management and contribute to significantly reducing water volumes used [18].

1.3.4 TinyML and Embedded Artificial Intelligence

The emergence of Tiny Machine Learning (TinyML) represents a major development in the field of smart agriculture. Unlike traditional approaches that require data processing in the cloud, TinyML allows machine learning models to be run directly on low-power microcontrollers [20].

The study by Taueatsoala et al. [20] demonstrates that integrating TinyML into smart irrigation systems improves device autonomy while reducing latency and dependence on internet connectivity. This approach also promotes reduced communication costs and improves the confidentiality of agricultural data.

Despite these advantages, several challenges remain, including limitations related to available memory, the computing power of microcontrollers, and the complexity of models that can be deployed on embedded platforms [20].

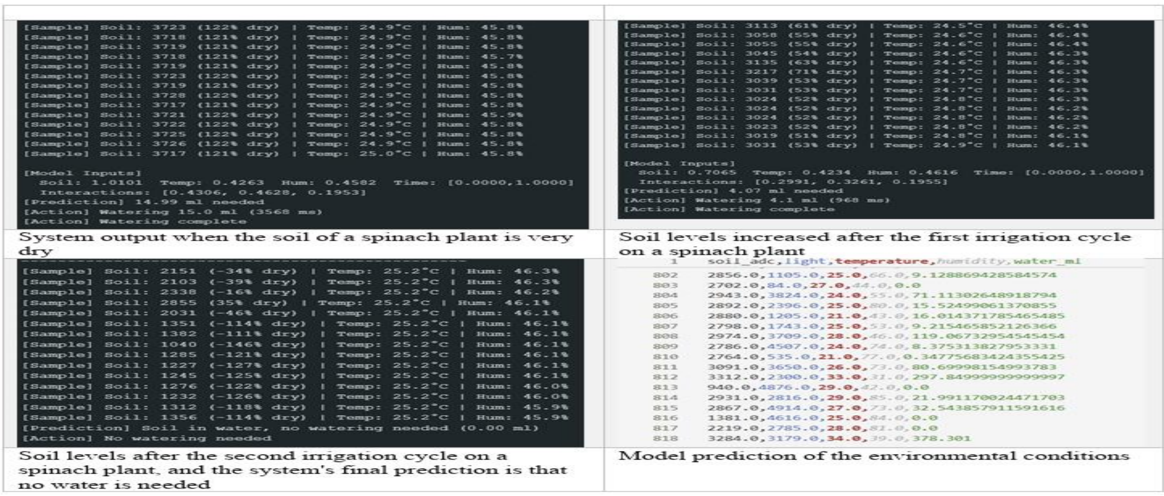

Figure 1.7: TinyML model training outputs [20].

1.3.5 Critical Analysis, Trends, and Perspectives of IoT-Based Smart Irrigation Systems

The analysis of the ten selected studies highlights the rapid evolution of smart irrigation systems based on the Internet of Things (IoT) and their contribution to more efficient water resource management. The proposed architectures rely primarily on the use of environmental sensors, particularly soil moisture sensors, combined with low-cost microcontrollers such as the ESP32, which appears to be the most widely adopted hardware platform due to its ease of integration, communication capabilities, and low deployment cost [12][16][19]. Most systems also utilize cloud platforms and mobile applications for remote monitoring and control of irrigation operations [13] [17].

A review of recent work reveals a gradual shift from conventional approaches based on fixed thresholds to smarter systems incorporating artificial intelligence techniques. These new approaches use algorithms capable of analyzing environmental data in real time and automatically adapting irrigation strategies to the actual needs of crops [20][22]. The introduction of methods such as fuzzy logic and Tiny Machine Learning (TinyML) further improves the accuracy of decisions while reducing energy consumption and dependence on cloud infrastructure [18][20]. The results reported by the various studies generally show a significant reduction in water consumption as well as an improvement in the operational efficiency of farms, thus confirming the potential of the IoT as a key technology for precision agriculture [13][15].

Despite these promising advances, several limitations remain in the current literature. The majority of the systems studied have been validated in experimental environments or on limited agricultural areas, which makes it difficult to evaluate their performance under real-world conditions on a large scale [16]. Furthermore, issues related to data security, cybersecurity of IoT infrastructures, communication reliability, and device energy autonomy remain insufficiently explored [13][20]. These challenges open the way to new research perspectives focused on integrating more advanced artificial intelligence models, developing higher-performing Edge Computing and TinyML solutions, and designing autonomous systems capable of operating efficiently in diverse agricultural environments [20][21].

Overall, recent literature demonstrates that IoT-based smart irrigation systems are a relevant solution for addressing current challenges in sustainable water management in agriculture. The convergence of IoT technologies, artificial intelligence, and low-power embedded systems suggests the future development of autonomous agricultural platforms capable of simultaneously improving productivity, environmental sustainability, and farm resilience to climate change [12][21].

1.4 Conclusion

This chapter reviewed recent developments in IoT-based smart irrigation systems and real-time monitoring technologies. The analyzed studies showed that most existing solutions rely on environmental sensors, ESP32-based platforms, wireless communication networks, and cloud services to automate irrigation processes and improve water resource management.

The literature review also highlighted the increasing integration of artificial intelligence, fuzzy logic, and TinyML techniques to enhance decision-making accuracy and optimize irrigation efficiency. These technologies contribute to reducing water consumption while improving agricultural productivity.

However, several limitations remain, particularly the dependence on Wi-Fi, GSM, or continuous internet connectivity, which restricts the deployment of such systems in remote agricultural areas. In addition, the processing capabilities of commonly used microcontrollers may limit the implementation of advanced monitoring and protection functions.

Therefore, there is a need for more reliable and autonomous irrigation systems capable of operating efficiently in rural environments. This motivates the development of the proposed system, which combines the TMS320F28379D controller, LoRa communication technology, and intelligent fault detection mechanisms to provide enhanced monitoring, protection, and irrigation management capabilities.

Chapter 2

Electrical Pump Motor Failures and Protection techniques including MATLAB /Simulink Modeling .

2.1 Introduction

Modern irrigation systems rely heavily on the use of electric pumps to transport and distribute water to cultivated areas. This equipment plays a vital role in improving agricultural productivity, particularly in regions where water resources are limited or subject to high climatic variability. However, the reliable and continuous operation of irrigation pumps is highly dependent on the quality of the power supply and the system's operating conditions [21].

The electric motors that drive the pumps are susceptible to several electrical and mechanical faults that can compromise their performance and reduce their lifespan. Among the most common electrical anomalies are overvoltage, undervoltage, voltage unbalance, overload, phase loss, and phase reversal. These defects can cause an excessive increase in current draw, abnormal heating of the windings, reduced energy efficiency, and, in the most severe cases, motor destruction [22][23].

Overvoltage generally leads to an increase in magnetic flux and ferromagnetic losses, which promotes motor heating. Conversely, undervoltage causes an increase in the current required to maintain the required mechanical torque, also resulting in winding overheating. Voltage imbalances between phases generate asymmetrical currents that create inverse sequence components, responsible for vibrations, additional losses, and a significant reduction in motor life [23][24].

Furthermore, hydraulic operating conditions can also lead to critical situations. Dry running, which occurs when the pump operates without water or with an insufficient water level, is one of the main causes of deterioration of mechanical seals, bearings, and hydraulic components. This condition can lead to a rapid increase in the pump's internal temperature and premature degradation of its components [24].

Faced with these risks, the implementation of appropriate protection and monitoring systems has become essential. Modern electronic protection relays enable the rapid detection of faults such as overvoltage, undervoltage, phase imbalance, overload, phase loss, phase reversal, and dry running. Their integration into irrigation systems helps improve operational reliability, reduce maintenance costs, and ensure the continuity of the water supply necessary for agricultural activities [22],[26].

Therefore, studying the various faults affecting irrigation pumps and the associated protection methods is a major challenge for optimizing equipment availability, enhancing energy efficiency, and ensuring the sustainability of modern irrigation systems.

2.2 Protection Methods for Electrical Disturbances and Abnormal Operating Conditions

2.2.1Over-Voltage

2.2.1.1 Definition of Overvoltage

Overvoltage is an abnormal condition of the electrical network characterized by a rise in the supply voltage above the specified motor rating. In irrigation pumping systems, overvoltage can result from variations in the electrical network, incorrect transformer settings, switching phenomena, or transient disturbances. This voltage increase causes a rise in magnetic flux in the motor's magnetic circuit, leading to increased iron losses, higher operating temperature, and a reduction in the insulation life of the windings [26][22].

For three-phase induction motors, prolonged overvoltage can also lead to magnetic circuit saturation, increased vibration, and reduced energy efficiency. When overvoltage exceeds the permissible limits defined by international standards, continuous motor operation becomes dangerous and can lead to premature equipment failure [27].

2.2.1.2 Calculating the Overvoltage Percentage

The overvoltage percentage is determined by comparing the measured voltage to the motor's rated voltage. It is calculated using the following equation:

$$OV(\%) = \frac{V_m - V_r}{V_r} \times 100$$

where:

Measured_V: actual voltage applied to the motor (V);

Rated_V: rated voltage indicated on the motor's nameplate (V).

<u>Example:</u>

For a motor rated at 400 V supplied with 440 V:

Overvoltage Percentage = [(440 − 400) / 400] × 100 = 10%

The motor is therefore subjected to an overvoltage of 10%.

2.2.1.3. Accepted Overvoltage Limits According to Motor Standards

IEC 60034-1 defines the operating limits of electric motors based on variations in mains voltage and frequency. Under normal operating conditions, a motor must be able to operate correctly when the supply voltage remains within ±5% of its rated value, while maintaining its rated performance [27].

The standard also specifies an extended operating range of up to ±10% of the rated voltage. Within this range, the motor can continue to operate, but certain characteristics such as temperature rise, efficiency, power factor, and torque may be affected [27][28].

When Is Overvoltage Acceptable?

Overvoltage is generally considered acceptable in the following situations:

- Voltage between +5% and +10% of the rated value.
- Limited exposure time.
- Motor temperature remaining within prescribed limits.
- Current drawn below the maximum permissible current.
- No abnormal vibrations or noise.
- Within this range, the motor can operate without immediate damage, although monitoring is recommended to prevent gradual insulation degradation [22][28].

When is overvoltage no longer acceptable?

Overvoltage becomes unacceptable when:

- The voltage exceeds +10% of the rated value.
- The condition persists for a prolonged period.
- The winding temperature exceeds the insulation thermal class.
- Magnetic saturation occurs.
- Excessive losses and heating are observed.

Under these conditions, the risk of insulation degradation, reduced motor life, and pump system failure increases significantly. For this reason, surge protection relays are generally set between 105% and 110% of the nominal voltage according to the manufacturer's recommendations and the application requirements [26][27].

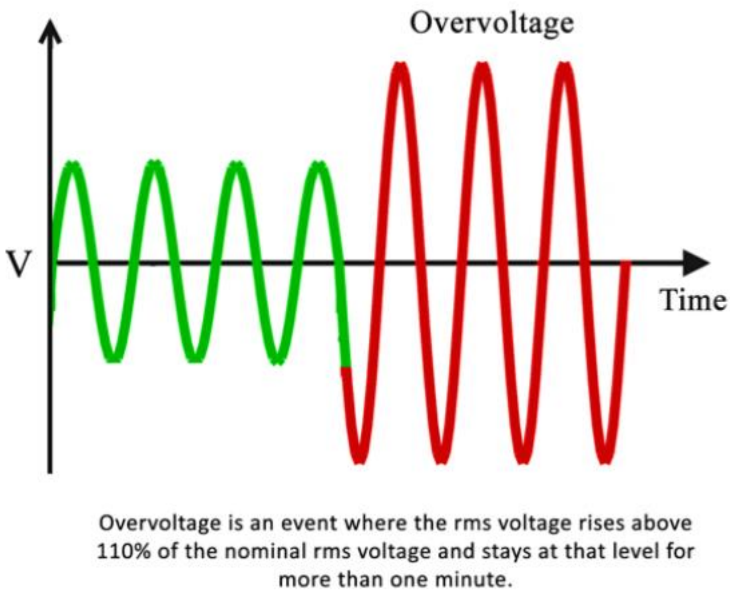

Figure 2.1: Healthy state and Over-Voltage signal [29]

2.2.2Under-Voltage

2.2.2.1 Definition of Under-Voltage

Undervoltage is an abnormal condition of the electrical network characterized by a decrease in the supply voltage below the motor's rated value. This phenomenon can be caused by network overload, excessive voltage drops in the cables, an undersized transformer, or faults in the electrical distribution system [29].

In induction motors used for irrigation pumps, undervoltage leads to a decrease in magnetic flux and motor torque. In order to maintain the mechanical power demanded by the load, the motor draws a higher current, which causes an increase in the winding temperature. Prolonged exposure to undervoltage can accelerate insulation aging, reduce energy efficiency, and lead to frequent tripping of thermal protection devices [21] [27].

2.2.2.2 Calculating the Undervoltage Percentage

The undervoltage percentage is calculated by comparing the rated voltage to the actual voltage measured at the motor terminals.

The equation used is:

$$\text{UV}(\%) = \frac{V_{\text{nominal}} - V_{\text{measured}}}{V_{\text{nominal}}} \times 100$$

where:

- Vnominal: is the motor's nominal voltage (V).
- Vmeasured: is the actual voltage applied to the motor (V).

Example:

For a 400 V motor supplied with 360 V:

Under-voltage (%) =[(400 - 360) / (400) × 100].

Under-voltage (%) = 10%.

The motor is therefore operating with an under-voltage of 10%.

2.2.2.3 Accepted Under-voltage Limits According to Motor Standards

According to IEC 60034-1, electric motors must operate under their rated conditions when the supply voltage remains within a range of ±5% around the rated voltage [27].

The standard also defines an extended operating range of up to −10% of the rated voltage. Within this range, the motor can continue to operate, but certain characteristics such as starting torque, efficiency, power factor, and temperature rise may be affected [27]

For motors powering centrifugal pumps, undervoltage is particularly critical during startup because the available torque is proportional to the square of the supply voltage. A small voltage reduction can therefore lead to a significant decrease in motor torque [21].

<u>When Is Under-voltage Acceptable?</u>

Under-voltage is generally considered acceptable when:

- The voltage remains between −5% and −10% of the rated voltage.
- The duration of the event is limited.
- The current drawn remains within permissible limits.
- The winding temperature remains below the limit for the insulation class.
- The mechanical performance of the pumping system is not significantly affected.

Under these conditions, the motor can continue to operate without immediate risk of damage [21][27].

When is undervoltage no longer acceptable?

Under-voltage becomes unacceptable when:

- The voltage drops below −10% of the rated voltage.
- The motor draws excessive current for a prolonged period.
- The motor torque becomes insufficient to drive the load.
- The temperature rise exceeds permissible limits.
- Repeated tripping of the thermal protection devices is observed.

In these situations, the motor's lifespan can be significantly reduced due to accelerated insulation degradation and increased heat loss. For this reason, undervoltage protection relays are generally set between 85% and 90% of the rated voltage to prevent prolonged operation under hazardous conditions [33][36].

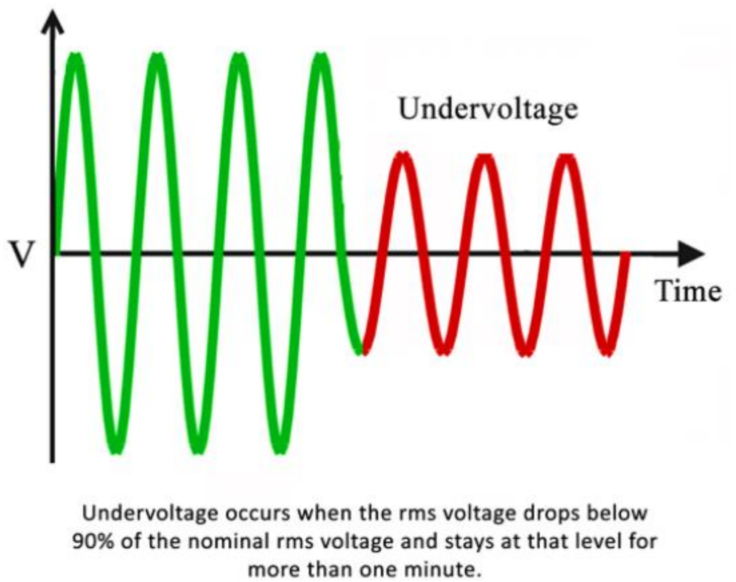

Figure 2.2: Healthy state and Under-Voltage signals [29]

2.2.3 Phase Loss

2.2.3.1 Definition of Phase loss

Phase loss, also called accidental single-phase operation, is an electrical anomaly that occurs when one of the three phases supplying a three-phase motor is interrupted while the other two phases remain energized. This situation can be caused by a blown fuse, a broken conductor, a poor connection in a circuit breaker, or a fault in the electrical network [30].

When a three-phase motor experiences phase loss during operation, it can continue to run thanks to the two remaining phases. However, this condition causes a significant current imbalance, a substantial increase in heat losses, and a significant reduction in motor torque. The currents in the two energized phases can reach 1.7 to 2 times their normal value, leading to rapid heating of the windings and a high risk of insulation damage [28][27].

If phase loss occurs during startup, the motor is generally unable to start and draws a current close to the stalled rotor current, which can lead to rapid motor failure without proper protection [21].

2.2.3.2 Phase Loss Detection and Calculation Method

Phase loss is not expressed as a percentage like overvoltage or undervoltage. It is usually detected by monitoring the voltages or currents of the three phases.

The phase loss condition is identified when:

$V_A = 0$ or $V_B = 0$ or $V_C = 0$

where:

V_A, V_B , V_C represent the voltages of the three phases.

Another method involves monitoring the currents:

$I_A = 0$ or $I_B = 0$ or $I_C = 0$

where:

I_A ,I_B ,I_C represent the currents of the three phases.

Modern protection relays typically detect phase loss when the voltage of one phase drops below 40% to 60% of its rated value for a predetermined duration [30].

2.2.3.3 Permissible Limits According to Motor Standards

According to IEC 60034-1 and motor protection standards, the complete loss of a phase is never considered a normal operating condition [27].

Unlike permissible voltage variations, no permanent tolerance is provided for operation with a missing phase. Three-phase motors are designed to operate with three balanced voltages, and the loss of one phase immediately results in a severe imbalance in the electrical system [39, 40].

Protection devices must detect this condition and disconnect the motor within a very short time to prevent thermal damage.

When is phase loss acceptable?

From a standards perspective, phase loss is never acceptable under steady-state conditions.

However, in some industrial installations, a very short detection delay is tolerated to prevent nuisance tripping due to transient network disturbances. This delay is generally between 1 and 5 seconds, depending on the application and the characteristics of the protection relay [30].

During this short period:

- The motor can remain powered.
- Currents increase rapidly.
- Thermal monitoring becomes essential.

When is phase loss no longer acceptable

Phase loss becomes immediately critical when:

- One phase is completely absent.
- The motor continues to operate under load.

- Currents exceed rated limits.
- The winding temperature rises rapidly.
- The motor torque becomes insufficient to drive the load.

Under these conditions, motor heating can be several times higher than normal operation. Without rapid intervention from the protection system, insulation degradation, an internal short circuit, or complete motor failure can occur within minutes [28]

For this reason, phase loss protection relays are systematically integrated into irrigation pumping systems to ensure the safety and reliability of electric motors.

2.2.4 The Unbalance

2.2.4.1 Definition of Unbalance

Unbalance in a three-phase system occurs when the voltages or currents of the three phases are not equal in magnitude and/or are not exactly 120° out of phase. In three-phase induction motors, this phenomenon leads to the appearance of negative sequence components, which cause increased current, additional losses, excessive heating, vibrations, and a reduction in motor life [31][32].

2.2.4.2 Voltage Imbalance Calculation

According to the NEMA MG-1 standard, the voltage imbalance percentage is calculated from the maximum deviation from the average voltage:

$$VU(\%) = \frac{\Delta V_{\text{max}}}{V_{\text{avg}}} \times 100$$

Where:

[Vavg = (VAB + VBC + VCA) / 3]

Example:

(VAB = 480V)

(VBC = 476V)

(VCA= 472V)

- **Average Voltage:**

Vavg= (480 + 476 + 472) / 3) = 476V

- **Maximum Deviation:**

Δ Vmax=4V.

- **Unbalance:**

Unbalance %=(4/476)100=0.84%.

This value is less than the generally recommended limit of 1% for normal motor operation [31][33].

2.2.4.3 Accepted Unbalance Limits According to Motor Standards

The generally accepted recommendations for three-phase motors are:

Unbalance ≤ 1%: normal operation, no power reduction required.

Unbalance between 1% and 2%: acceptable operation, but increased monitoring is recommended.

Unbalance between 2% and 5%: power reduction (derating) is necessary to prevent motor overheating.

Unbalance > 5%: operation not recommended; significant risk of overheating, vibration, and insulation degradation [31][32][34].

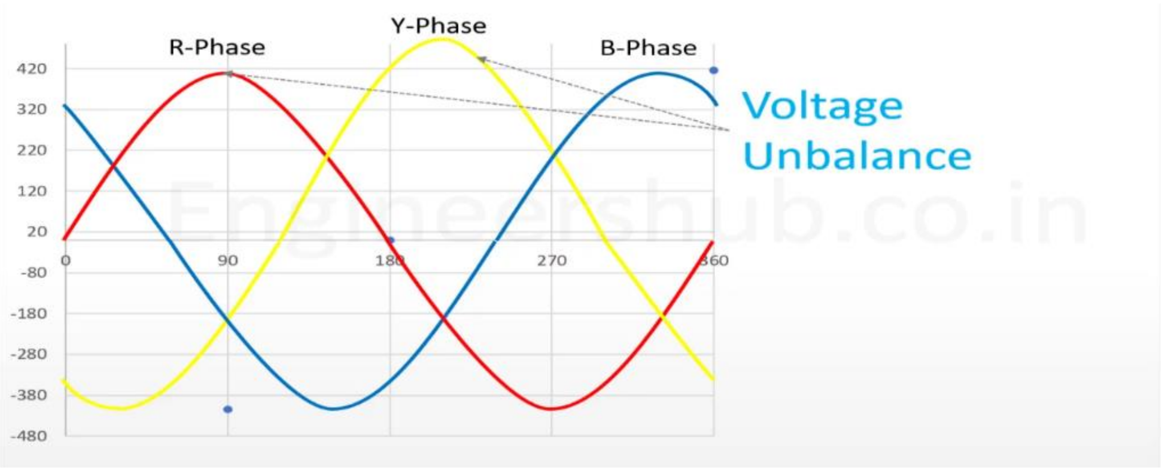

Figure 2.3: Voltage Unbalance signal [35]

2.2.5 The Overload

2.2.5.1. Definition of Overload

In the field of rotating electrical machines—motors and generators—overload refers to an operating condition in which the machine is subjected to loads exceeding its rated values: rated current, rated power, rated torque, or rated apparent power. It therefore corresponds to a situation where the electromechanical demand exceeds the capacity specified by the manufacturer for the operating condition in question.

Overload is primarily critical because it increases Joule losses, winding heating, insulation aging, and the risk of tripping or machine damage [36][37]. IEC 60034-1:2026 is the basic standard for the rated characteristics and performance of rotating electrical machines and supersedes the 2022 edition [36].

2.2.5.2 Calculating Overload from Current

An electrical machine overload occurs when its rated operating value is exceeded, generally expressed as current, power, or torque. For electric motors, the calculation using current is most commonly used, as the current drawn is directly related to winding heating and insulation degradation. [27][28]

Load Rate Equation:

$$\text{Load Rate}(\%) = \frac{I_{\text{measured}}}{I_{\text{rated}}} \times 100$$

Overload Percentage Equation:

$$\text{Overload}(\%) = \frac{I_{\text{measured}} - I_{\text{rated}}}{I_{\text{rated}}} \times 100$$

Or:

$$OL(\%) = LR(\%) - 100$$

Where:

Measured Current: the current actually drawn by the motor, in amperes (A).

Rated Current: the rated current indicated on the motor's nameplate, in amperes (A). [36].

Example:

If a motor has a rated current of 20 A and actually draws 24 A:

Overload (%) = [(24 − 20) / 20] × 100

Overload (%) = 20%

The motor is therefore operating at 120% of its rated load, which corresponds to an overload of 20%.This level of overload should not be considered acceptable in steady state, as it can lead to excessive heating and requires the intervention of appropriate thermal protection [37][39].

When power is used instead of current:

$$\text{Power Overload}(\%) = \frac{P_{\text{actual}} - P_{\text{rated}}}{P_{\text{rated}}} \times 100$$

When torque is used:

$$\text{Torque Overload}(\%) = \frac{T_{\text{actual}} - T_{\text{rated}}}{T_{\text{rated}}} \times 100$$

These methods are used when the overload is assessed from the mechanical power supplied or the torque demanded from the machine [36].

When the overload is acceptable?

1- The overload is acceptable when the measured current is less than or equal to the motor's rated current, that is, when measured current (I) ≤ rated current (I). In this case, the load is less than or equal to 100%, and this is not considered an actual overload [36].

2- A very slight overload, generally between 0% and 5%, may be tolerated only for a short period, provided that the motor temperature remains within permissible limits and that the operating conditions comply with the manufacturer's specifications. [36][38].

3- A temporary overload may be acceptable if explicitly provided for by the manufacturer, the motor's operating conditions, or the applicable standard. It must be limited in duration and must not cause excessive heating [36][38].

4- The overload may be considered acceptable if the thermal protection device is correctly set to the motor's rated current and if the tripping threshold is not reached under normal operating conditions. [37][39].

When overload is not acceptable?

1- Overload is not acceptable when the motor operates continuously above its nominal current. Continuous operation with measured current (I) > nominal current (I) results in increased Joule losses and heating. [36][38]

2- An overload between 5% and 20% is not acceptable under steady-state conditions. It must be considered an abnormal condition requiring monitoring or load correction. [36][38]

3- An overload of 20% or more, i.e., when the measured current (I) is ≥ 1.20 × nominal current (Inominal), is considered unacceptable for continuous operation. In this case, the thermal overload relay or protective device must normally provide the tripping protection according to its tripping class. [37][39]

4- A high overload, for example, close to 50%, i.e., a measured current (I) ≈ 1.50 × nominal current (Inominal), can only be accepted as an exceptional and very temporary condition. It must never be considered a steady-state operating condition. [36][37]

5- Overload is not acceptable if it causes excessive temperature, accelerated aging of the insulation, repeated tripping, reduced efficiency, or a risk of machine damage. [36][38].

Situation Overload Percentage Interpretation

- 1.05 I nominal < I measured < 1.20 I nominal 5% to 20% Actual overload; unacceptable under steady-state conditions. [36][39]
- I measured ≥ 1.20 I nominal ≥ 20% Unacceptable overload; the protective device must activate according to its settings. [37][39]
- I measured ≈ 1.50 I nominal ≈ 50% Significant overload; permissible only for a very short period if authorized by the standard or manufacturer. [36][37]

Repeated or Continuous Overload Variable Unacceptable, as it reduces the insulation lifespan and increases the risk of failure. [36][38]

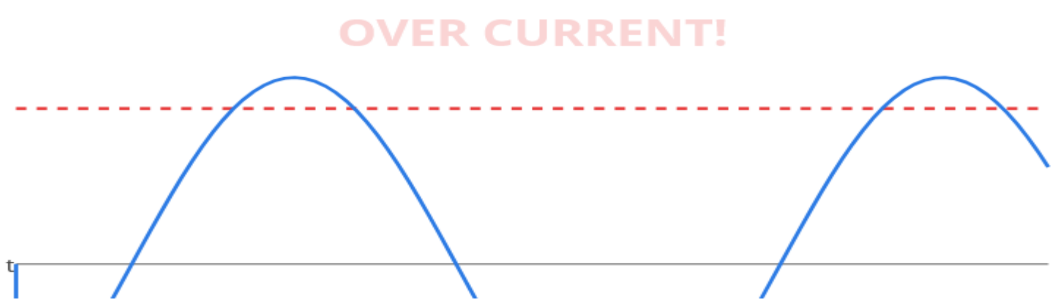

Figure 2.4: Over Current and Current Threshold [40]

2.2.6 Phase Reversal

2.2.6.1 Definition of Phase Reversal

Phase reversal, also called phase reversal or phase sequence reversal, is an electrical fault that occurs when the normal phase sequence of a three-phase system is reversed. In a balanced three-phase network, the phase sequence is usually L1–L2–L3 (ABC). A phase reversal occurs when two phases are swapped, resulting in a reversed sequence, for example, L1–L3–L2 (ACB) [41].

In rotating electrical machines, particularly three-phase induction motors, this reversal causes an immediate change in the direction of the rotating magnetic field. Consequently, the motor rotates in the opposite direction to that intended, which can lead to mechanical damage to coupled equipment such as pumps, fans, conveyors, or compressors [21].

2.2.6.2 Phase Reversal Detection and Calculation

1-The most common method for detecting a phase reversal involves analyzing the timing sequence of zero crossings of the three phase voltages. If the order of the crossings is:

VA→VB→VC the sequence is considered normal (ABC).

However, if the order becomes:

VA→VC→VB a phase reversal is detected [55].

2- A method based on voltage vectors consists of calculating the sign of the following determinant:

$$D = \begin{vmatrix} V_A & \sin(\theta_A) & \cos(\theta_A) \\ V_B & \sin(\theta_B) & \cos(\theta_B) \\ V_C & \sin(\theta_C) & \cos(\theta_C) \end{vmatrix}$$

Where:

θA, θB et θC represent the phase angles. A change in the sign of D indicates a phase reversal [55].

2.2.6.3 Regulatory Requirements

Phase reversal protection is recommended in industrial installations in accordance with the safety and motor protection principles described in IEC 60204-1, concerning the safety of electrical equipment in machinery, and in IEC 60034, which deals with rotating electrical machines. These standards recommend the implementation of phase sequence monitoring devices to prevent starting in the wrong direction of rotation and the associated mechanical damage [43][42].

2.2.7 Dry Running

2.2.7.1 Definition of Dry Running

Dry running refers to an abnormal condition in which an electric pump continues to operate even though no liquid, or an insufficient amount of liquid, is present at its inlet. This situation typically occurs due to a lack of water in the reservoir, a low well level, a blockage in the suction line, or a leak in the hydraulic circuit [25].

In pumping systems driven by three-phase induction motors, dry running significantly reduces the load torque applied to the motor shaft. As a result, the motor draws less current than its rated current. Prolonged exposure to this condition can lead to overheating of the mechanical seals, premature wear of the bearings, and pump failure [44].

2.2.7.2 Dry Run Detection and Calculation

The most common method in motor protection systems is to monitor the current drawn by the motor. When the pump is operating normally, the current is close to its rated load. During dry run, the current drops significantly due to the reduction in mechanical load [41].

The motor load percentage can be estimated by:

$$\text{Charge } (\%) = \frac{I_{\text{mesuré}}}{I_{\text{nominal}}} \times 100$$

where:

Imeasured is the measured RMS current;

Inominal is the rated current indicated on the motor's nameplate.

The percentage of dry running can then be defined as:

$$\text{Dry Running } (\%) = \left(1 - \frac{I_{\text{mesuré}}}{I_{\text{nominal}}}\right) \times 100$$

This relationship allows us to assess the load reduction compared to nominal conditions.

2.2.7.3 Detection threshold according to industry practices

IEC standards for electrical machines do not specify a universal value for the dry running threshold, as this depends on the type of pump and its application. However, industry recommendations indicate that dry running is generally suspected when the current drawn drops to between 60% and 80% of the nominal current for a predefined period [41][27].

For a motor with a rated current of:

In=3.4A a typical detection threshold of 70% corresponds to:

Idry=0.7×3.4=2.38A

Thus, if the measured RMS current remains below 2.38 A for several seconds, dry running can be declared.

2.2.7.4 Normative Considerations

Underload protection is the standardized method for detecting dry running in pumping systems. General motor protection requirements are described in IEC 60034 standards for rotating electrical machines and in the recommendations for industrial motor protection published by leading electrical equipment manufacturers [27][45].

2.3 Simulation and Validation of Pump Motor Fault Detection and Protection Using MATLAB/Simulink

MATLAB/Simulink provides a powerful environment for modeling, analyzing, and validating electrical systems before their practical implementation. In this work, MATLAB/Simulink was used to develop and evaluate the proposed diagnostic and protection system for three-phase pump motors operating under various abnormal electrical conditions.

The developed simulation model reproduces the operating behavior of the pump motor and continuously monitors the electrical quantities required for fault detection. Different fault scenarios were investigated, including over-voltage, under-voltage, phase loss, voltage unbalance, overload, phase reversal, and dry-running conditions. For each fault, the corresponding detection logic and protection actions were verified to ensure reliable operation.

The simulation stage plays an important role in validating the effectiveness of the proposed diagnostic system before hardware implementation. It allows the verification of fault detection thresholds, relay response, and overall system behavior under different operating conditions. Furthermore, simulation reduces development cost and time while providing a safe environment for testing fault situations that may be difficult or hazardous to reproduce experimentally.

2.3.1 Modeling and Simulation of the Proposed Diagnostic System

Figure 2.5 illustrates the MATLAB/Simulink model of the proposed diagnostic and protection system developed for three-phase pump motors. The model integrates voltage and current monitoring blocks, fault detection algorithms, threshold comparison units, and relay control logic to evaluate the system response under different operating conditions.

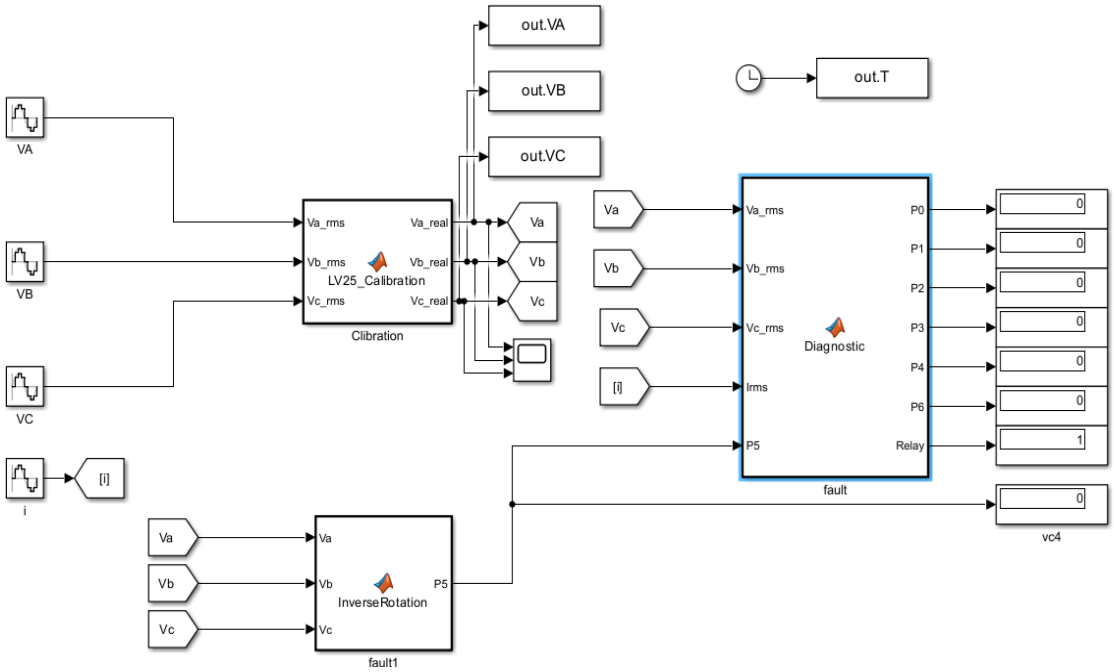

Figure 2.5: MATLAB/Simulink Model of the Proposed Diagnostic System

In this stage of the project, MATLAB/Simulink R2025a is employed to develop and validate the proposed diagnostic and protection system for three-phase pump motors. The simulation environment provides a safe and flexible platform for analyzing system behavior under normal and fault conditions before hardware implementation.

The proposed system integrates multiple protection functions within a unified diagnostic framework, thereby reducing the need for conventional protection devices such as overload relays, phase sequence relays, and phase monitoring relays. The performance of the system is evaluated under various fault conditions, including over-voltage, under-voltage, phase loss, voltage unbalance, overload, phase reversal, and dry-running. The practical implementation of the proposed system and the associated diagnostic algorithms are described in Chapter 3.

NB: In the simulation model, the relay operates according to active-low logic. A logic value of **1** corresponds to the healthy operating state, while a logic value of **0** indicates a detected fault and activates the protection relay.

A- Over-voltage Detection

In the healthy operating condition, the voltage sensors measure a nominal phase voltage of **220 V**, which is considered suitable for normal motor operation. Under this condition, the fault signal remains inactive and the protection relay is not triggered.

Based on standard over-voltage protection practices, the over-voltage threshold is set at **10% above the rated voltage**. Therefore, if any of the three-phase voltages exceeds **242 V**, the system identifies an over-voltage fault and generates a trip signal to activate the protection relay, thereby preventing potential damage to the motor.

Figure 2.6 presents the MATLAB/Simulink model configured for the over-voltage fault condition. The figure shows the voltage acquisition blocks, the diagnostic subsystem, and the relay output used to detect and respond to the fault.

The corresponding voltage waveforms are illustrated in **Figure 2.7**. It can be observed that one phase voltage reaches **242 V**, exceeding the nominal value of **220 V**, while the remaining phases continue to operate at their normal levels. Once the over-voltage threshold is exceeded, the diagnostic system detects the abnormal condition and issues the appropriate fault indication.

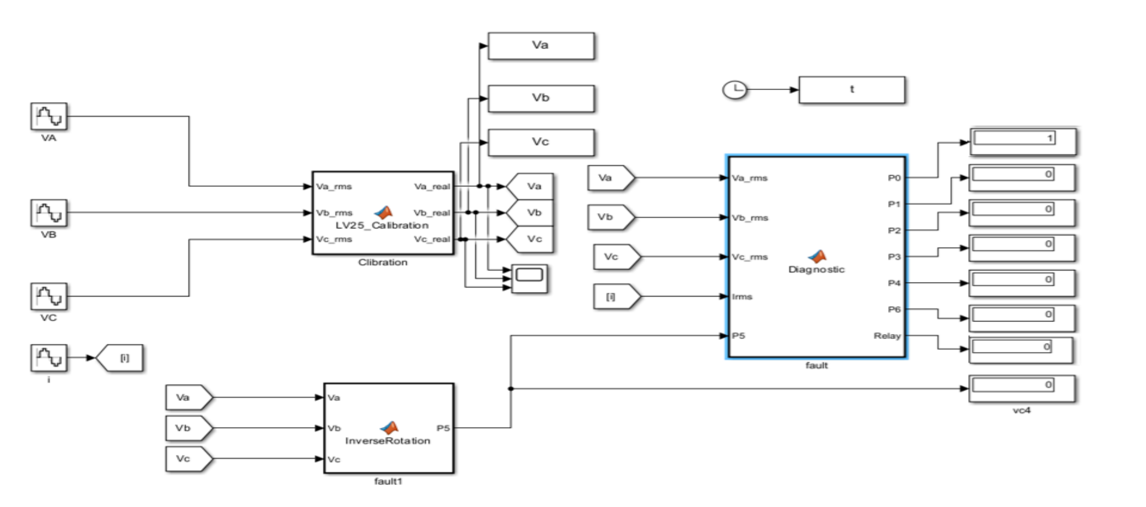

Figure 2.6: Over-Voltage state of the system

Figure 2.7: Three-Phase Voltage Signals during Over-Voltage Detection

B- Under-voltage Detection:

Based on under-voltage protection standards, the under-voltage threshold is set at **5% below the rated voltage**. Therefore, a voltage level of **209 V** is considered the minimum acceptable operating voltage, and any voltage below this threshold will trigger the protection relay.Under normal operating conditions, the three-phase voltages remain at their nominal value of **220 V**, ensuring proper motor operation. In this healthy state, no fault is detected and the protection relay remains inactive.

Figure 2.8 illustrates the MATLAB/Simulink model configured to simulate an under-voltage fault condition. The diagnostic subsystem continuously monitors the three-phase voltages and compares them with the predefined threshold value. The corresponding voltage waveforms are presented in **Figure 2.9**. It can be observed that phase **VB** drops below the normal operating voltage and reaches approximately **209 V**, while phases **VA** and **VC** remain at their nominal values. Once the measured voltage falls below the under-voltage threshold, the diagnostic system identifies the fault condition and generates a fault signal to activate the protection relay.

As a result, the motor is disconnected from the power supply, preventing excessive current draw, overheating, and potential damage caused by prolonged operation under under-voltage conditions.

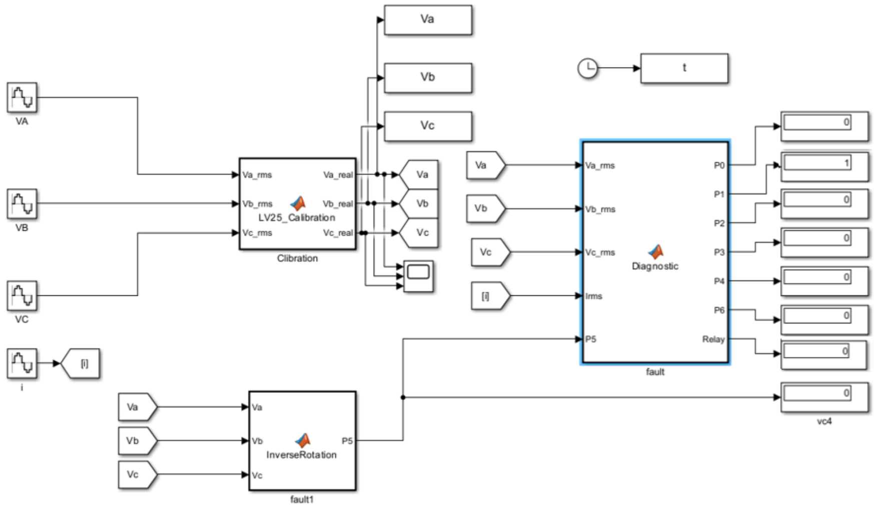

Figure 2.8: Under-Voltage state of the system

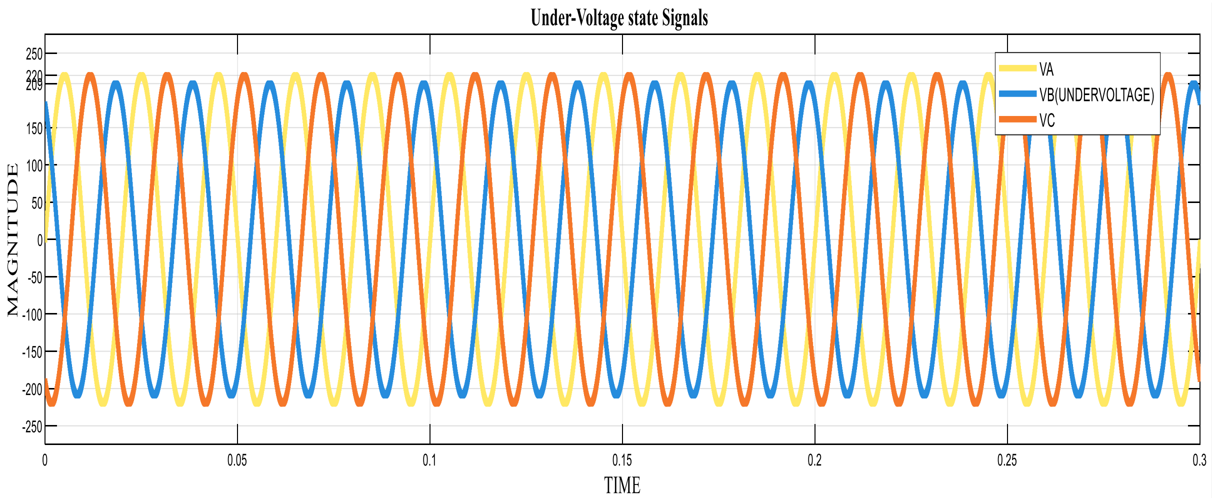

Figure 2.9: Under-Voltage state Signals

C- Phase Loss Detection :

According to phase loss detection standards, the phase loss threshold is set at **132 V**. When the voltage of any phase falls below this value, the diagnostic system detects a phase loss fault and generates a fault signal. **Figure 2.10** shows the MATLAB/Simulink model used to simulate this condition.

The corresponding voltage waveforms are presented in **Figure 2.11**, where phases **VA** and **VB** remain at their nominal voltage of **220 V**, while phase **VC** decreases to **132 V**. Once the threshold is reached, the protection relay is activated to disconnect the motor and prevent damage caused by prolonged phase loss operation.

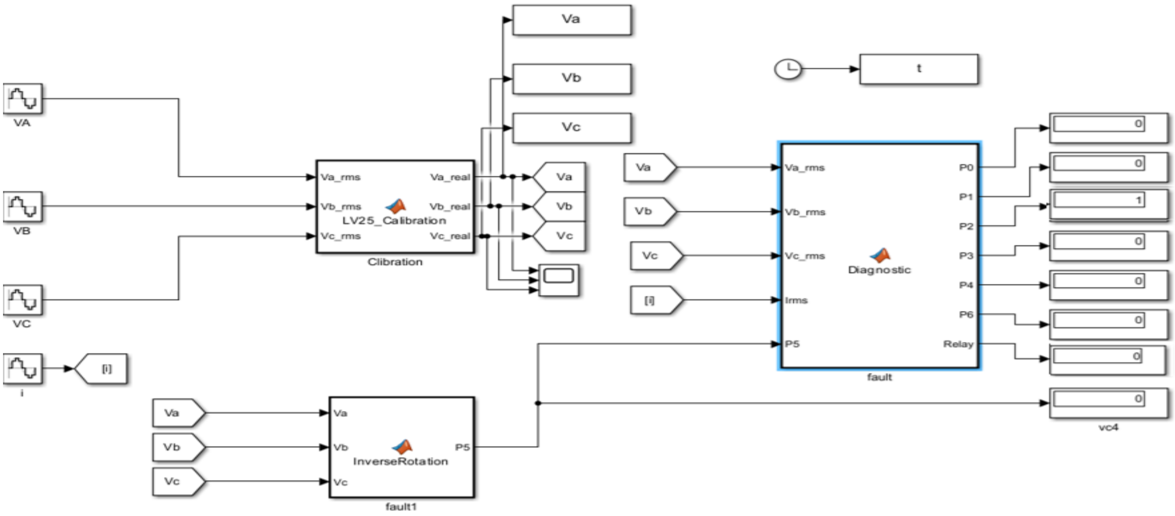

Figure 2.10: Phase Loss state of the system

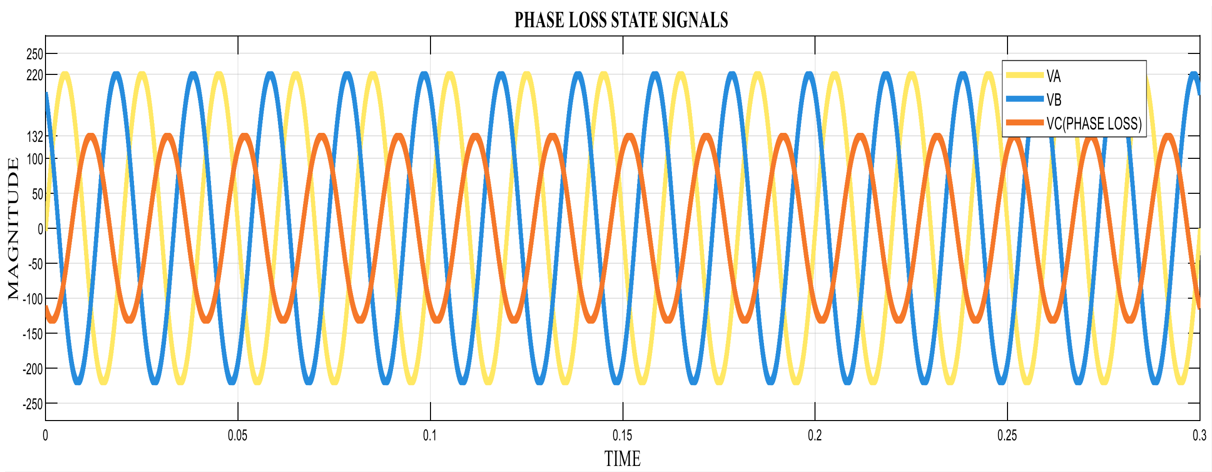

Figure 2.11 : Phase Loss state signals

D- Unbalance Detection:

Based on voltage unbalance standards, the unbalance threshold is set at **5%**. The mathematical verification confirms an unbalance level of **5%**, validating the fault condition. **Figure 2.12** shows the MATLAB/Simulink model used to simulate the voltage unbalance fault, while **Figure 2.13** presents the corresponding three-phase voltage waveforms with unequal amplitudes. Once the unbalance exceeds the predefined threshold, the diagnostic system detects the fault and activates the protection relay to protect the motor from abnormal operating conditions.

The Math Check:

Average: $V_{avg} = \frac{203.5+228.25+228.25}{3} = \frac{660}{3} = \mathbf{220V}$

Deviations:

- $d_1 = |203.5 - 220| = \mathbf{16.5V}$
- $d_2 = |228.25 - 220| = \mathbf{8.25V}$
- $d_3 = |228.25 - 220| = \mathbf{8.25V}$

Unbalance: $\text{Max Deviation} = 16.5\text{V}$

$$\text{Unbalance} = \frac{16.5 \times 100}{220} = \mathbf{5.00\%}$$

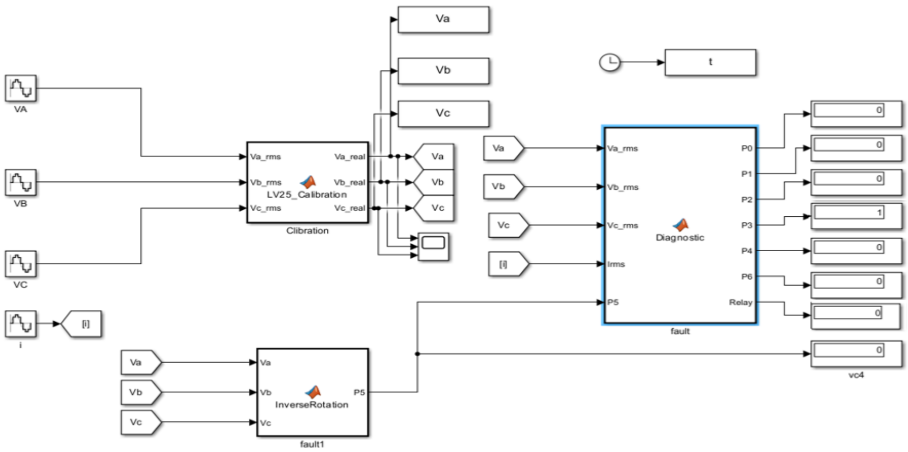

Figure 2.12: Unbalance state of the system

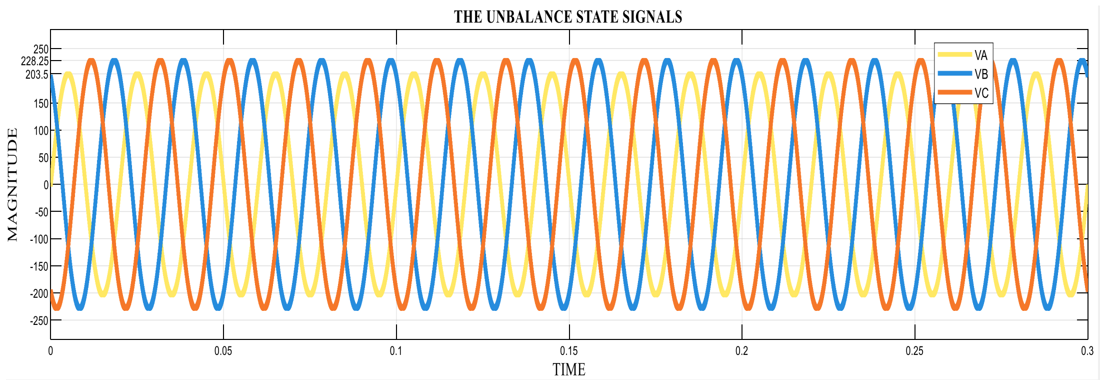

Figure 2.13: Unbalance state signals

E- Overload Detection :

According to overload protection standards, the trip threshold is set at **1.25 times the rated current (3.4 A)**. Therefore, the protection relay is activated when the current reaches **4.25 A**. **Figure 2.14** shows the MATLAB/Simulink model used to simulate the overload condition and evaluate the response of the proposed diagnostic system.

The corresponding current waveforms are presented in **Figure 2.15**, where the overload current exceeds the reference current of **3.4 A** and reaches the threshold value of **4.25 A**. Once this limit is exceeded, the diagnostic system detects the overload condition and generates a fault signal, causing the protection relay to disconnect the motor and prevent overheating and possible damage to the motor windings.

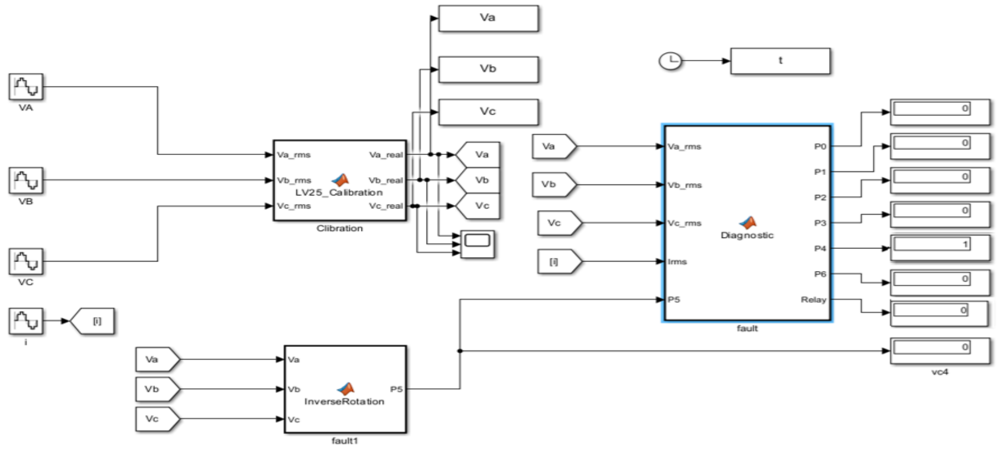

Figure 2.14: Overload state of the System

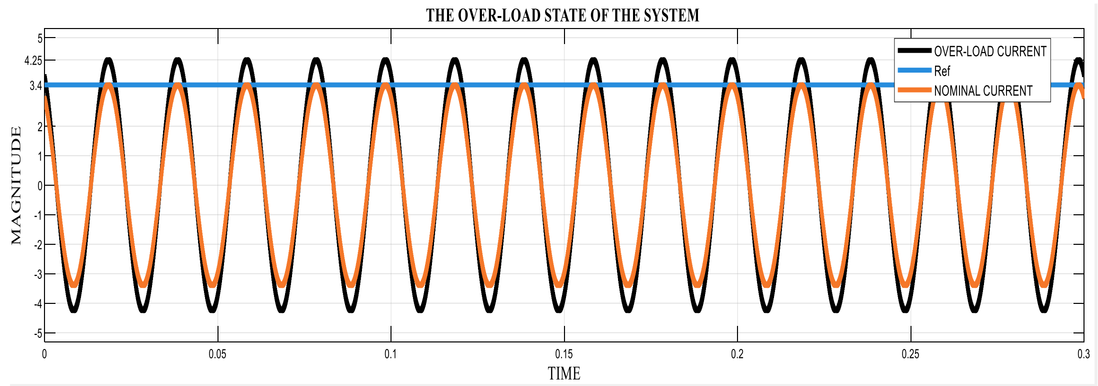

Figure 2.15: Overload state signals

F- Phase Reversal Detection:

The normal phase sequence of a three-phase system is **L1–L2–L3 (ABC)**. A phase reversal fault occurs when two phases are interchanged, resulting in a reversed phase sequence and consequently reversing the motor rotation direction. **Figure 2.16** illustrates the MATLAB/Simulink model used to simulate the phase reversal condition and evaluate the response of the proposed diagnostic system.

The corresponding voltage waveforms are shown in **Figures 2.17(a)** and **2.17(b)**. **Figure 2.17(a)** presents the healthy operating condition with the normal phase sequence (ABC), whereas **Figure 2.17(b)** shows the phase reversal condition after two phases have been swapped. Once the abnormal phase sequence is detected, the diagnostic system generates a fault signal and activates the protection relay to prevent reverse motor rotation and potential damage to the pumping system.

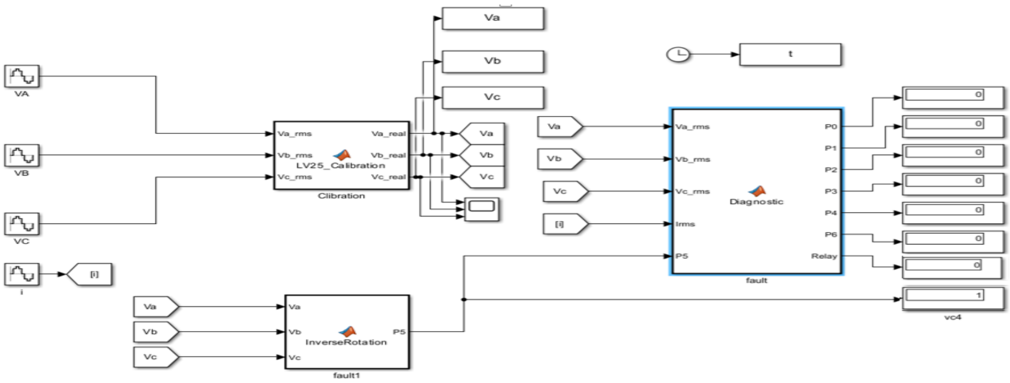

Figure 2.16 : The Phase Reversal state of the System

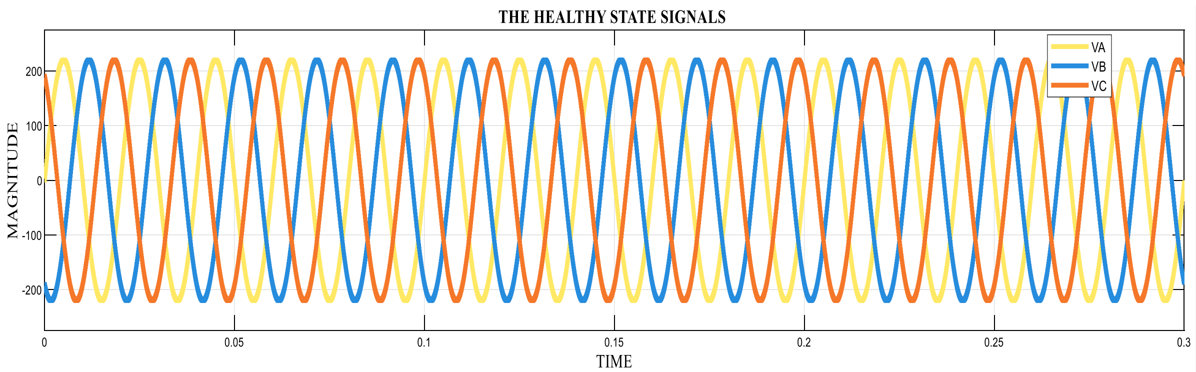

Figure 2.17.A: The healthy state signals

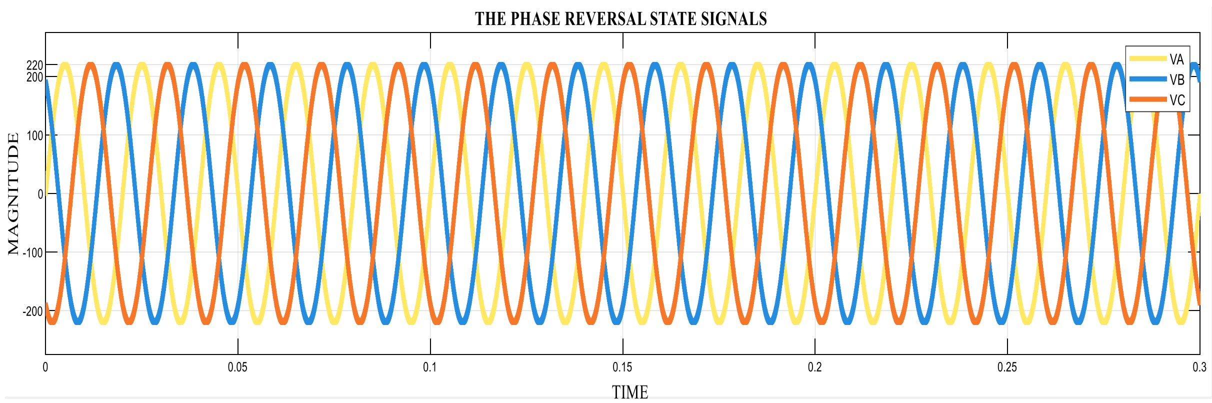

Figure 2.17.B: The phase reversal state signals

G- Dry Running Detection:

According to industry standards, a dry-running condition is generally identified when the motor current decreases to between **60% and 80% of its nominal value**. In this study, the dry-running threshold is set at **2.72 A**, corresponding to **80% of the nominal current (3.4 A)**.

Figure 2.18 shows the MATLAB/Simulink model used to simulate the dry-running condition and evaluate the response of the proposed diagnostic system. The diagnostic subsystem continuously monitors the motor current and compares it with the predefined threshold value.

The corresponding current waveforms are presented in **Figure 2.19**, where the operating current decreases from the nominal value of **3.4 A** to **2.72 A**, indicating a dry-running condition. Once the current falls below the specified threshold, the diagnostic system detects the fault and generates a fault signal, causing the protection relay to disconnect the motor. This protection prevents damage to the pump and motor that may result from prolonged operation without sufficient water flow.

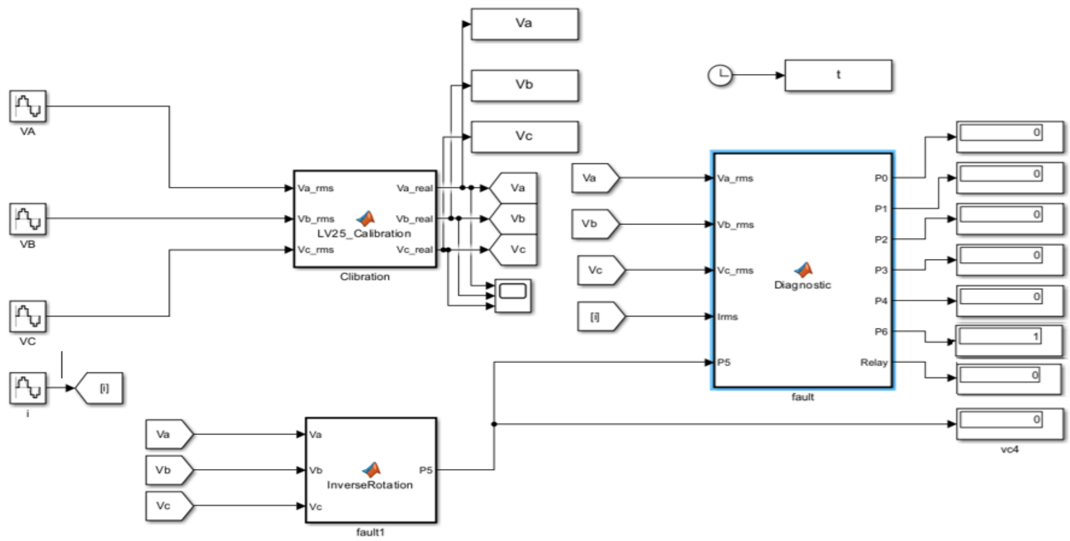

Figure 2.18: Dry Running state of the system

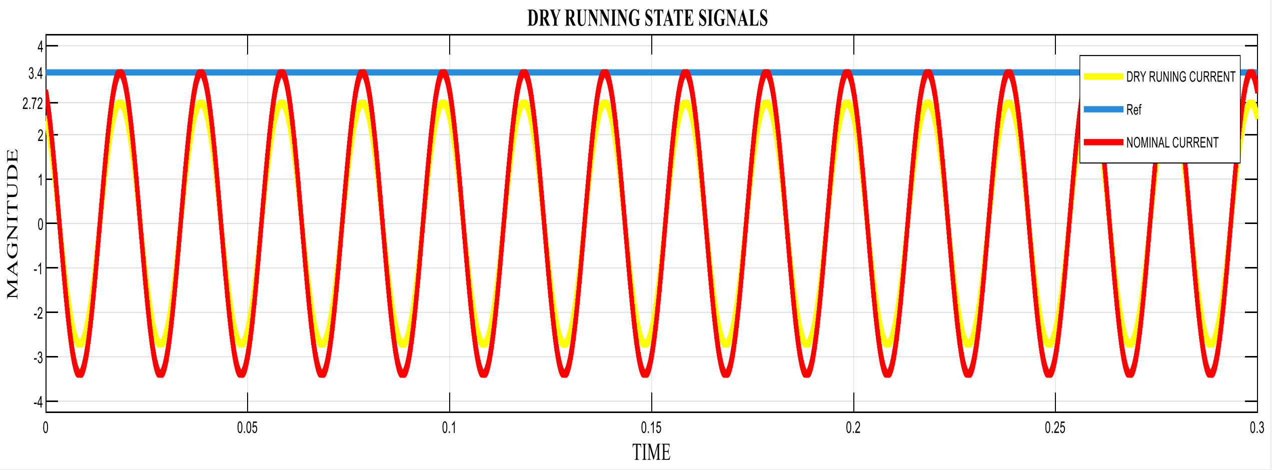

Figure 2.19: Dry Running state signals.

2.4 Conclusion

The results obtained through simulations performed using MATLAB/Simulink R2025a in conjunction with C2000 libraries validated the operation and performance of the proposed intelligent diagnostic system. The various operating scenarios studied demonstrated the system's ability to effectively detect the seven faults considered in this study: overvoltage, undervoltage, voltage imbalance, overload, phase loss, phase reversal, and dry running.

The simulation results show that the system is capable of analyzing measured electrical signals in real time, including three-phase voltages and currents, to accurately identify the operating state of the installation. Thanks to the developed monitoring and diagnostic algorithms, it is possible to reliably distinguish between a normal operating state (healthy state) and a degraded or faulty state (malfunctioning state).

Furthermore, this simulation phase provided a thorough understanding of the system's behavior under various operating conditions and allowed for verification of the relevance of the detection criteria selected for each type of fault. The observed performance confirms the potential of this approach to replace several conventional protection devices with a single, intelligent, and scalable solution.

Thus, the results obtained constitute an essential step before the practical implementation of the system on the chosen hardware platform. They demonstrate the

feasibility of the proposed approach and provide a solid foundation for the experimental development and real-time validation that will be presented in the following chapters.

Chapter 3
Real-Time Fault Diagnosis and Protection of Water Pump Motors Using the TMS320F28379D Microco-ntroller.

3.1 Introduction

Irrigation is a crucial element of modern agricultural development. It plays a vital role in improving crop productivity, managing water resources efficiently, and ensuring food security. In many agricultural regions, particularly those with variable climates or low rainfall, irrigation systems are essential for stable and sustainable agricultural production.

However, farmers face Plenty of challenges daily related to the operation and maintenance of irrigation systems. Electrical failures in pump motors, such as overvoltage, undervoltage, voltage imbalance, overload, phase loss, phase reversal, or dry running, can lead to service interruptions, production losses, and significant maintenance costs. These difficulties are particularly pronounced in rural and isolated areas, where Wi-Fi and GSM network coverage is often limited or non-existent, making it difficult to implement conventional remote monitoring solutions.

To address these Issues, this chapter details the proposed intelligent irrigation system. This solution is based on the integration of an advanced fault diagnostic system capable of detecting and identifying, in real time, the main anomalies affecting the pump motors. Data processing and decision-making are handled by the TMS320F28379D real-time microcontroller, whose high performance enables continuous monitoring and rapid response to fault conditions.

Furthermore, the system utilizes LoRa (Long Range) technology to ensure data transmission over long distances without requiring internet access, Wi-Fi, or GSM coverage. This approach guarantees a reliable, cost-effective solution adapted to rural environments, while ensuring the continuity of irrigation system operation and the protection of pumping equipment.

In this chapter, we will describe the general architecture of the proposed system, the various hardware and software modules used, as well as the strategies implemented for the monitoring, diagnosis and intelligent protection of irrigation installations.

3.2 System Architecture

The proposed intelligent irrigation system is based on the TMS320F28379D microcontroller, which serves as the system's central processing unit. This microcontroller is responsible for the real-time acquisition and analysis of the pump motor's electrical parameters by measuring three phase voltages and a line current.

To perform this data acquisition, the system uses three LV25-P voltage sensors and one LA25-NP current sensor. These sensors continuously monitor electrical quantities and transmit their analog signals to the TMS320F28379D microcontroller, where the processing, diagnostic, and protection algorithms are executed.

To ensure remote monitoring of the installation, the system incorporates two ESP32 boards. The first is connected to the TMS320F28379D microcontroller via the UART communication protocol, thus enabling the transfer of acquired data and diagnostic information. This same ESP32 board then communicates with a second ESP32 board using LoRa (Long Range) technology, ensuring reliable data transmission over long distances without requiring a Wi-Fi connection or GSM coverage. This architecture allows for a permanent link between the irrigation system and the farmer via their mobile phone.

Thanks to this solution, the user can view the motor's voltage and current values in real time, while also receiving instant notifications if an anomaly or malfunction is detected. In addition, the system is equipped with a protection relay controlled directly by the TMS320F28379D microcontroller. When a fault is identified by the diagnostic system, this relay automatically disconnects the pump from its power supply to prevent damage, ensure the safety of the installation, and guarantee continuous irrigation service under optimal conditions.

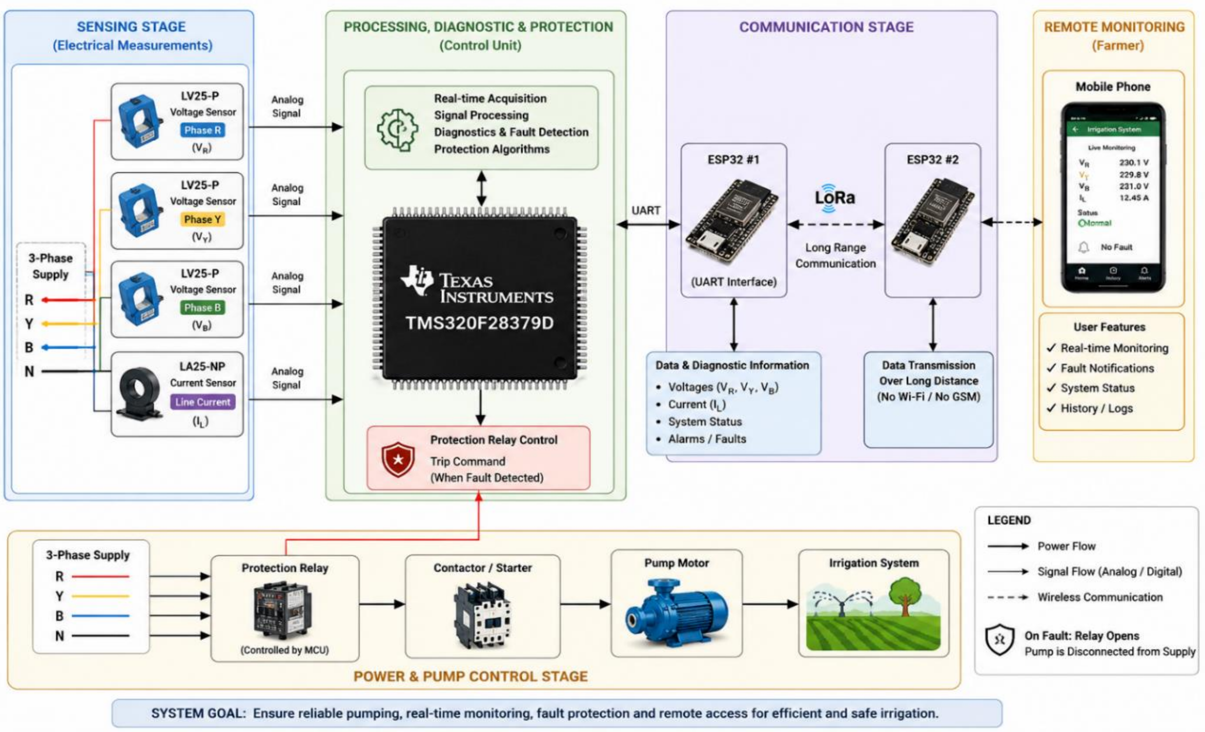

Figure 3.1: The System Architecture

3.3 Hardware Components and Functional Roles

3.3.1 Current Sensor (LA25-NP)

Figure 3.2: Current Sensor LA25-NP [46]

The LA 25-NP is a closed-loop, Hall-effect current transducer manufactured by LEM. It is designed to safely and precisely measure AC, DC, and pulsed currents (up to 36A) while providing complete galvanic isolation between the high-power primary circuit and low-voltage control electronics. [46]

3.3.1.1 Technical Specifications (LA25-NP)

I_{PN} Primary nominal RMS current 25 At

I_{PM} Primary current, measuring range 0 … ±36 At

R_M Measuring resistance @		T_A = 70 °C		T_A = 85 °C	
		$R_{M\,min}$	$R_{M\,max}$	$R_{M\,min}$	$R_{M\,max}$
with ±15 V	@ ±25 At max	100	320	100	315 Ω
	@ ±36 At max	100	190	100	185 Ω

I_{SN} Secondary nominal RMS current	25 mA
N_P/N_S Turns ratio	1-2-3-4-5 : 1000
U_C Supply voltage	(±5 %) ±15 V
I_C Current consumption	10 + I_S mA

[46]

3.3.2 Voltage Sensor (LV25-P)

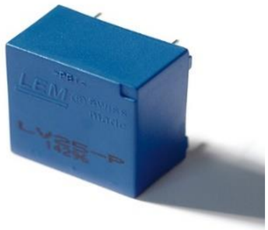

Figure 3.3: Voltage Sensor LV25-P [46]

The LEM LV 25-P is a closed-loop (compensated) voltage transducer based on the Hall effect. Unlike the LA 25-NP model, which directly measures a high current, the LV 25-P is designed to measure voltages (AC, DC, or pulsed) from 10 V to 500 V by converting the input voltage into a small, proportional current.

3.3.2.1 Technical Specifications (LV25-P)

I_{PN} Primary nominal RMS current		10		mA	
I_{PM} Primary current, measuring range		0 … ±14		mA	
R_M Measuring resistance		R_{Mmin}	R_{Mmax}		
with ±12 V	@ ±10 mA max	30	190	Ω	
	@ ±14 mA max	30	100	Ω	
with ±15 V	@ ±10 mA max	100	350	Ω	
	@ ±14 mA max	100	190	Ω	
I_{SN} Secondary nominal RMS current		25		mA	
N_P/N_S Turns ratio		2500 : 1000			
U_C Supply voltage (±5 %)		±12 … 15		V	
I_C Current consumption		10 (@ ±15 V) + Is		mA	[46]

3.3.3 Filtering and shifting circuits

To ensure accurate acquisition of AC voltage and current signals using the LA25-NP and LV25-P sensors, appropriate signal-conditioning stages are required. These stages include low-pass filtering circuits to attenuate high-frequency noise and level-shifting circuits to adapt the sensor outputs to the input range of the ADC. The selected component values and circuit configurations provide effective noise reduction and proper signal biasing, ensuring reliable and precise measurements by the TMS320F28379D microcontroller.

The LA25-NP and LV25-P sensors are powered by a symmetrical ±15 V supply to ensure proper operation. Their measurement terminals are connected to the electrical quantities being monitored, with a maximum rating of 250 V for voltage and 10 A for current. The analog output (M) of each sensor is then fed into a low-pass filter circuit, which removes high-frequency noise and unwanted disturbances to produce a cleaner and more stable signal. Since the measured quantities are alternating current (AC), the resulting signals contain both positive and negative values; therefore, a level-shifting stage is required to add a suitable DC offset so that the signal becomes entirely positive and compatible with the analog-to-digital converter. After filtering and shifting, the signal is conditioned and scaled to remain within or TMS320F28379D, ensuring accurate and reliable measurement acquisition.

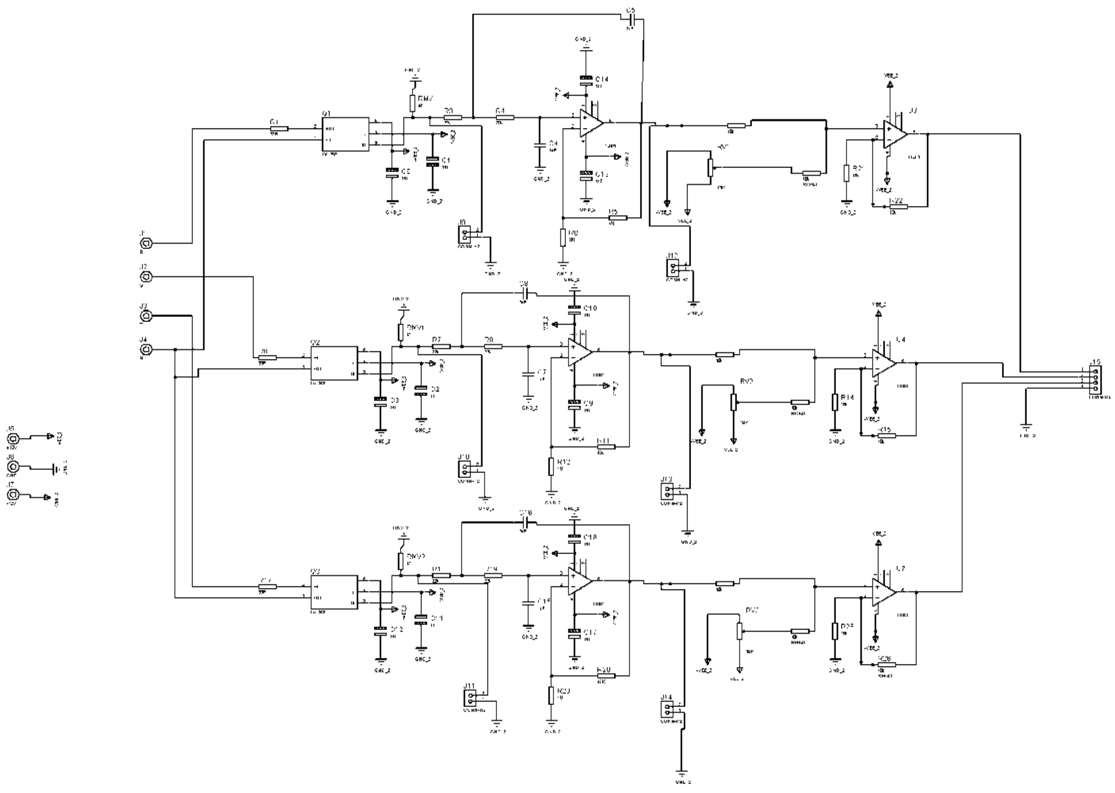

Figure 3.4: schematic of Voltage sensors

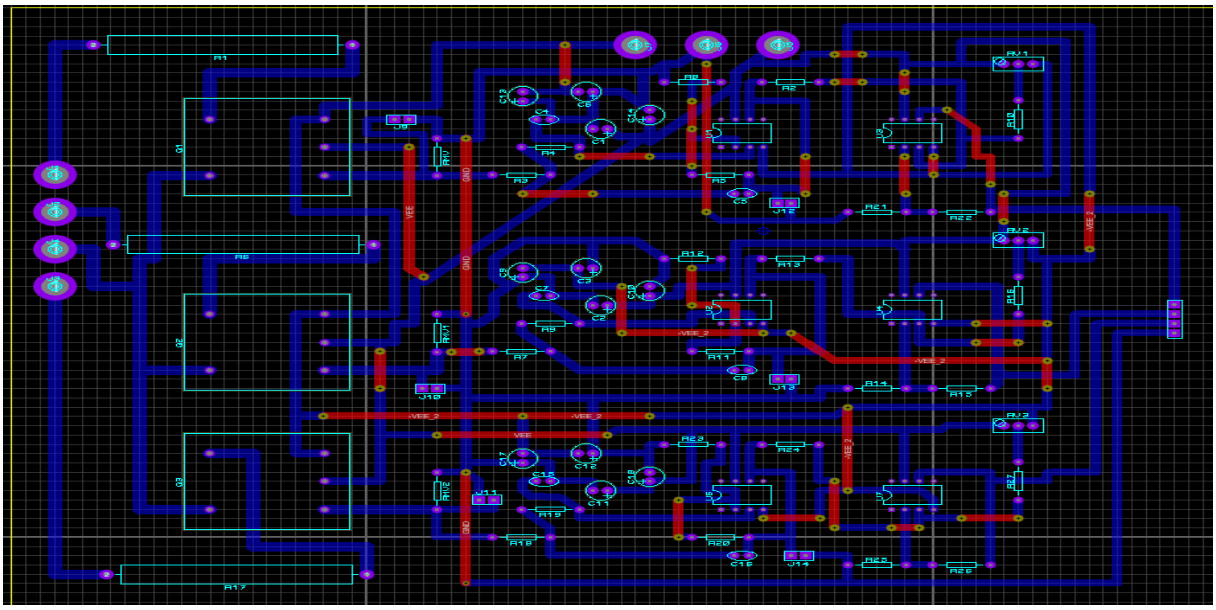

Figure 3.5: PCB of Voltage sensors

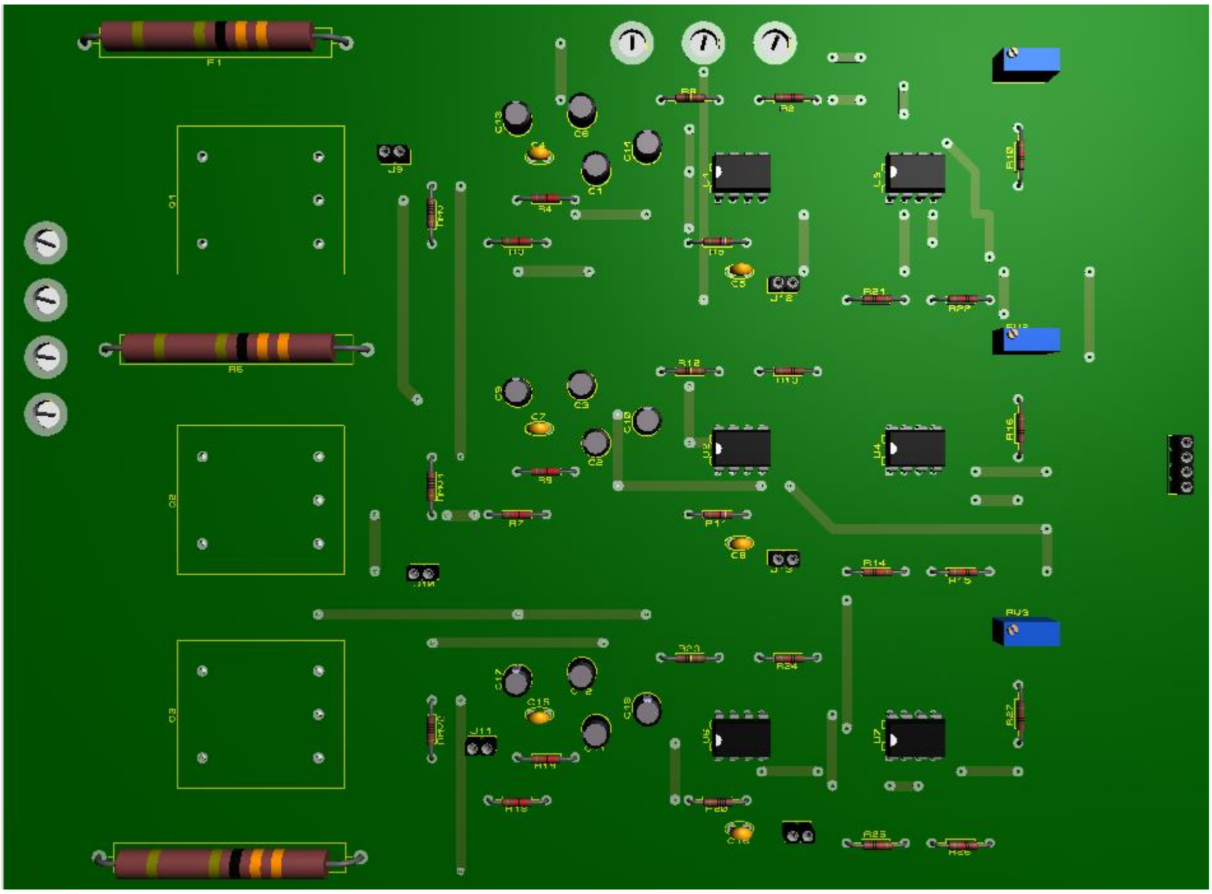

Figure 3.6: 3D PCB of Voltage sensors

The following figures illustrate the different stages of PCB design for voltage sensors:

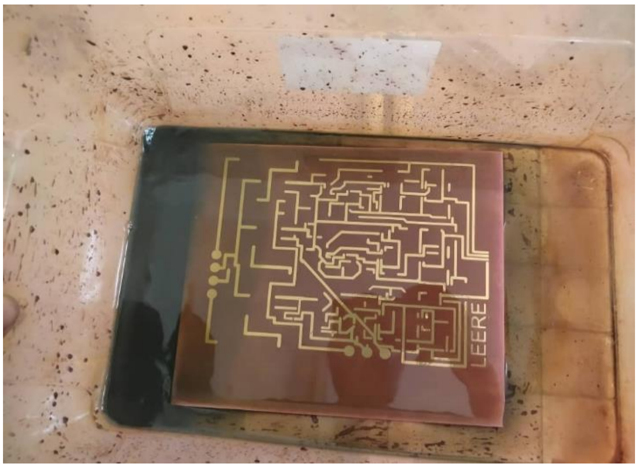

Figure 3.7: The PCB is submerged in ferric chloride

This step is called: Chemical etching of the printed circuit board (PCB). It involves removing unwanted copper from the board, leaving only the circuit traces. This is done by immersing the board in a ferric chloride ($FeCl_3$)solution, which attacks and dissolves the exposed copper.

Before this step, adhesive paper (or transfer paper/PCB special paper) is generally used to define the circuit. The trace pattern is first printed and then transferred onto the copper board. The areas protected by the adhesive paper or mask resist etching, while the unprotected areas are removed by the chemical etching solution.

Thus, after etching, only the circuit traces corresponding to the electronic design remain as shown in the following figure .

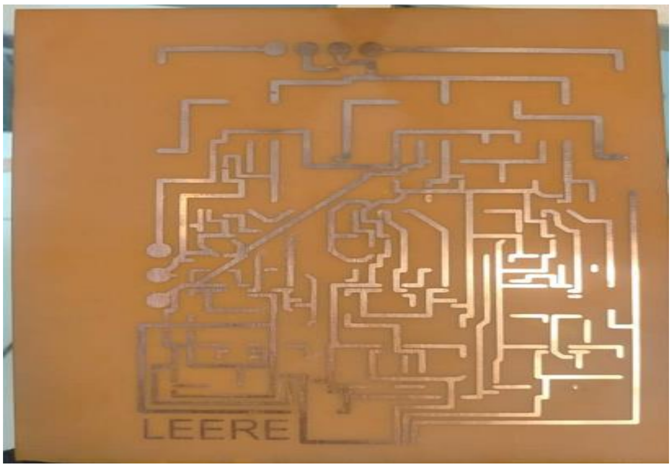

Figure 3.8: The PCB after exposed to ferric chloride

After this, the PCB is ready for drilling and soldering the components, and the final result is shown in the following figure.

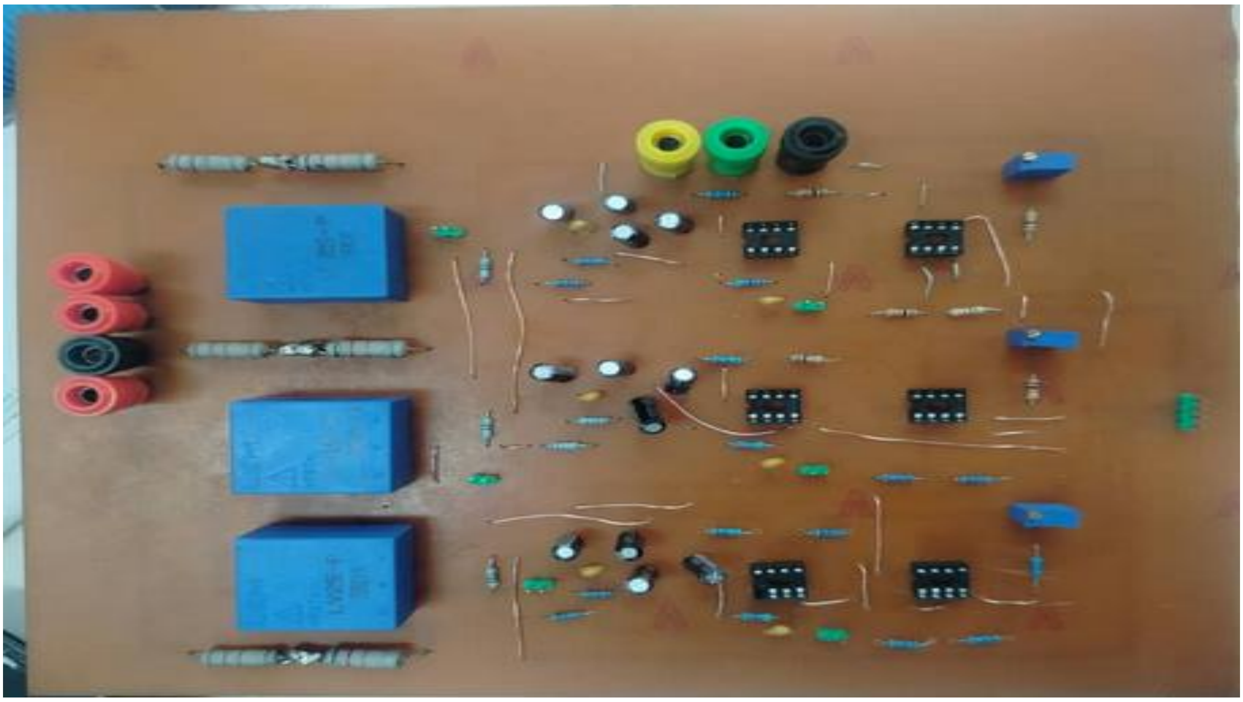

Figure 3.9: The PCB is ready to be used

And for current sensor, we use the following schematic:

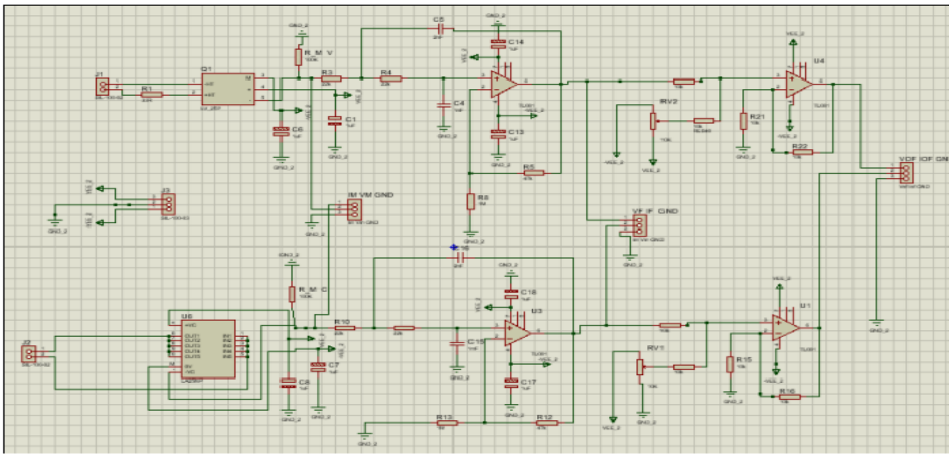

Figure 3.10: Schematic of current sensor

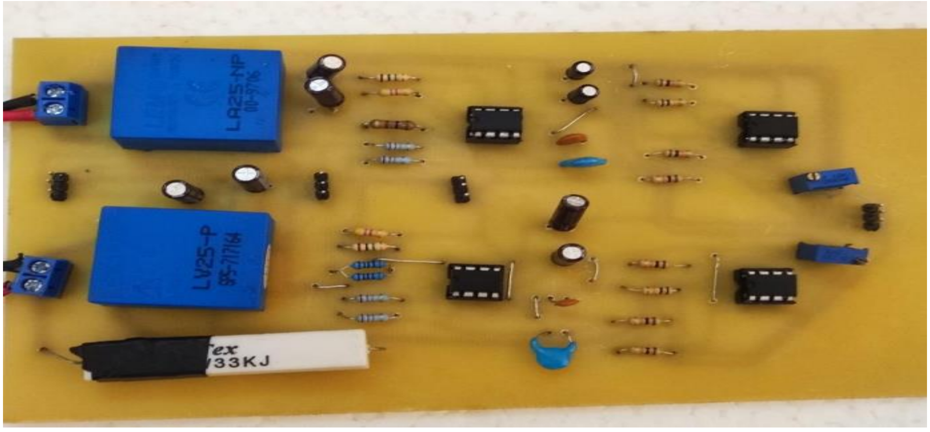

Figure 3.11: The PCB of current sensor

3.3.4 C2000 Microcontroller Lunchpad TMS320F28379D

The TMS320F28379D is a real-time microcontroller from the C2000™ Delfino™ family developed by Texas Instruments. It is designed for applications requiring high computing power and fast execution of control algorithms, particularly in power electronics systems, static converters, electric motor drives, and smart grids. This component integrates two TMS320C28x cores operating at a maximum frequency of 200 MHz, thus providing high performance for industrial and embedded applications [49].

The microcontroller features significant onboard memory, including up to 1 MB of Flash memory and 204 KB of RAM, enabling the implementation of complex signal processing and real-time control algorithms. It also integrates several communication interfaces such as SPI, I²C, SCI (UART), CAN, and USB, facilitating its integration into industrial control and supervisory architectures [49].

One of the key strengths of the TMS320F28379D lies in its advanced analog subsystem. It features four analog-to-digital converters (ADCs) capable of operating with 12-bit or 16-bit resolution, enabling fast and accurate acquisition of voltage and current signals. This feature is particularly important in electrical system monitoring and control applications where measurement accuracy is critical .

Furthermore, the TMS320F28379D integrates up to 24 PWM (Pulse Width Modulation) outputs as well as HRPWM (High-Resolution PWM) modules, providing high resolution for generating control signals. These features make it particularly well-suited for controlling inverters, DC-DC converters, and drive systems, where the quality of PWM signals directly influences system performance [49].

Thanks to all these features, the TMS320F28379D is a high-performance and widely used solution in advanced numerical control and power electronics applications .

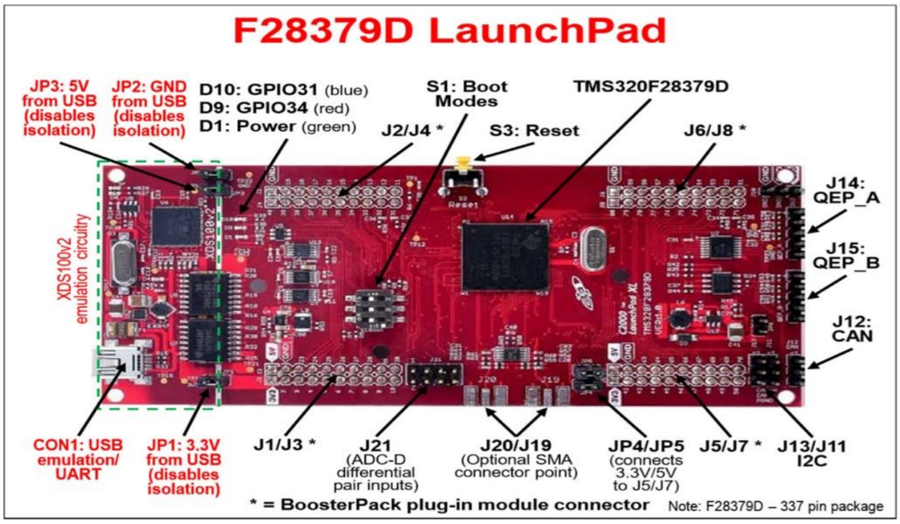

Figure 3.12: F28379D Launchpad with Technical specifications

3.3.5 ESP32-WROOM-32

The ESP32-WROOM-32 is a Wi-Fi and Bluetooth module developed by Espressif Systems. Based on the ESP32 chip, it is widely used in Internet of Things (IoT), industrial automation, home automation, and embedded systems applications due to its low power consumption, wireless communication capabilities, and low cost [47].

The module integrates a dual-core 32-bit Xtensa® processor capable of operating at up to 240 MHz, providing sufficient performance for the simultaneous execution of control, communication, and data processing tasks. It also features integrated SRAM and external Flash memory, typically ranging from 4 MB to 16 MB depending on the module version [47].

One of the key features of the ESP32-WROOM-32 is its native integration of Wi-Fi 802.11 b/g/n and Bluetooth v4.2 (BR/EDR and BLE) technologies. This dual connectivity enables data exchange with remote equipment, mobile applications, or real-time monitoring platforms.

Thanks to these features, the module is particularly well-suited for remote monitoring, telemetry, and control systems [47].

The ESP32-WROOM-32 also features a large number of configurable input/output pins (GPIO) and several communication interfaces such as UART, SPI, I²C, I²S, CAN (TWAI), and PWM. It also integrates 12-bit analog-to-digital converters (ADCs) for acquiring analog signals from various sensors. These features facilitate its integration into measurement, control, and data acquisition projects [47].

Thanks to its computing power, integrated wireless connectivity and hardware flexibility, the ESP32-WROOM-32 module is a high-performance solution for the development of connected embedded systems and IoT applications requiring reliable communication and local data processing [47].

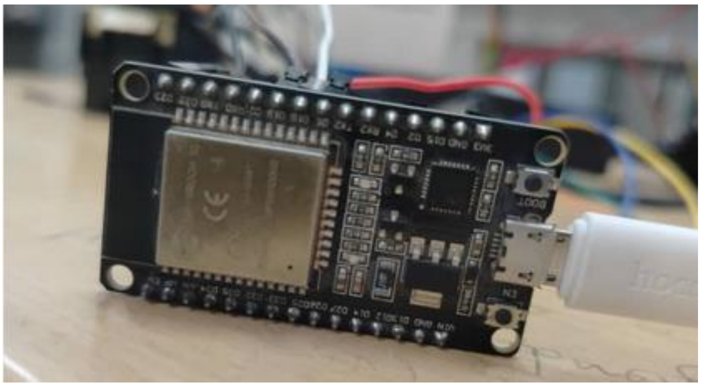

Figure 3.13: ESP32 WROOM-32 Board

3.3.6 LoRa SX1278

The SX1278 is a radio transceiver developed by Semtech Corporation and designed for long-range, low-power wireless communication applications. It incorporates LoRa (Long Range) technology, which enables data transmission over several kilometers while maintaining low power consumption. Thanks to these features, the SX1278 is widely used in Internet of Things (IoT) applications, telemetry, wireless sensor networks, smart agriculture, and remote monitoring systems [48].

The SX1278 operates primarily in the 137 MHz to 525 MHz frequency bands, particularly around 433 MHz, which is frequently used in many countries for industrial, scientific, and medical (ISM) applications. The LoRa modulation employed by this component is based on

Chirp Spread Spectrum (CSS), which significantly improves communication robustness against noise and interference while increasing transmission range [48].

This integrated circuit offers a receive sensitivity of up to −148 dBm, enabling it to detect extremely weak signals. Combined with a transmit power of up to +20 dBm, this high sensitivity allows for communication over several kilometers in open environments. The SX1278 also supports the classic FSK, GFSK, MSK, and OOK modulation schemes, providing high flexibility to meet application requirements [48].

Communication with a microcontroller is via an SPI (Serial Peripheral Interface), facilitating integration with platforms such as the ESP32, Arduino boards, or Texas Instruments' C2000 family of microcontrollers. The component also features several hardware error detection mechanisms, including Cyclic Redundancy Check (CRC) and Forward Error Correction (FEC), which contribute to improved transmission reliability

Thanks to its long range, low power consumption and high robustness against electromagnetic interference, the SX1278 is a particularly suitable solution for remote data monitoring and communication systems requiring reliable operation in wide-area environments [48].

Figure 3.14: LoRa SX1278

3.3.7 The Mobile APP

The developed system is based on an IoT architecture composed of three main elements: a mobile application installed on the phone, a web server and an ESP32 card connected to a TMS320F28379D microcontroller. The mobile application serves as a user interface for system monitoring and control, allowing the user to view the motor status and send start or stop commands via a simple interface (START/STOP buttons).

When a command is sent from the application, it is transmitted to the web server, which acts as an intermediary between the user and the embedded system. The ESP32 regularly polls this server to retrieve control orders, then activates a relay to start or stop the motor accordingly. In parallel, the ESP32 receives electrical measurements (voltages and current) in real time from the TMS320F28379D via UART communication, then transmits them to the server for storage and remote viewing on the mobile application.

Thus, the system ensures both real-time monitoring and remote control of the Machine thanks to continuous communication between the mobile application, the web server (http://iotmoteur.atwebpages.com/card.php) and the ESP32 on-board unit.

Figure 3.15 : The Monitoring Mobile App

3.4 The results and discussion

To evaluate the efficiency of the system and validate the results obtained in the previous simulation stage, the system was tested under real operating conditions, take in count all the previously studied faults.

3.4.1 The Voltage and Current PCB'S

Initially, we tested the voltage and current PCB boards to verify if the signals are correctly filtered and shifted.

We used an oscilloscope to visualize the signals. The results obtained are as follows:

3.4.1.1 The voltage sensors PCB : (VA,VB,VC)are completely identical

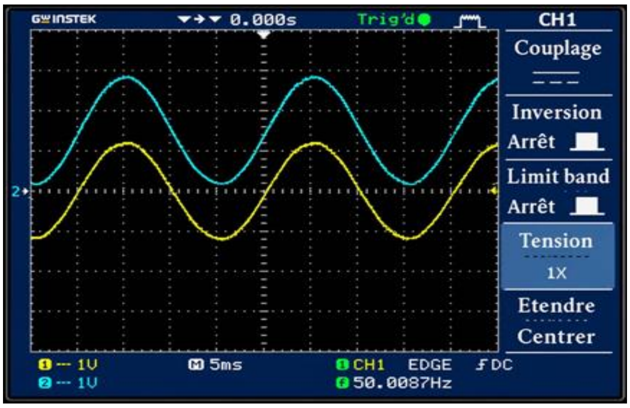

Figure 3.16 : The Voltage sensors signals

As we can see, the three voltage sensors exhibit identical amplitudes, both for the filtered signals (in yellow) and for the offset signals (in blue). We also observe that the offset circuits are functioning correctly, since the signals are entirely above 0 V and remain below 3.3 V. This voltage range corresponds to the configuration required for proper acquisition by the analog inputs (ADCs) of the LaunchPad TMS320F28379D (C2000) board.

4.1.2 The Current sensor PCB

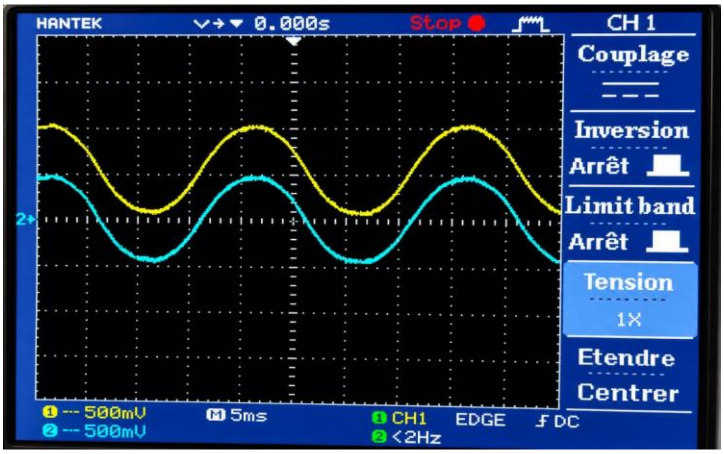

Figure 3.17 : The Current sensor signals

As we can see, the current sensor PCB provides the desired signals: the filtered signal (in blue) and the shifted signal (in yellow).

3.4.2 The last test of the system

We conducted a final practical test under real-world conditions before implementing the IoT control and monitoring system. We used GPIO outputs P0 through P6 for fault signaling, and output P8 for the fault relay. GPIOs P0 through P6 are connected to LEDs, with P0 corresponding to the rightmost LED, and so on. This allows for clear identification of faults that occur when the protection relay is triggered.

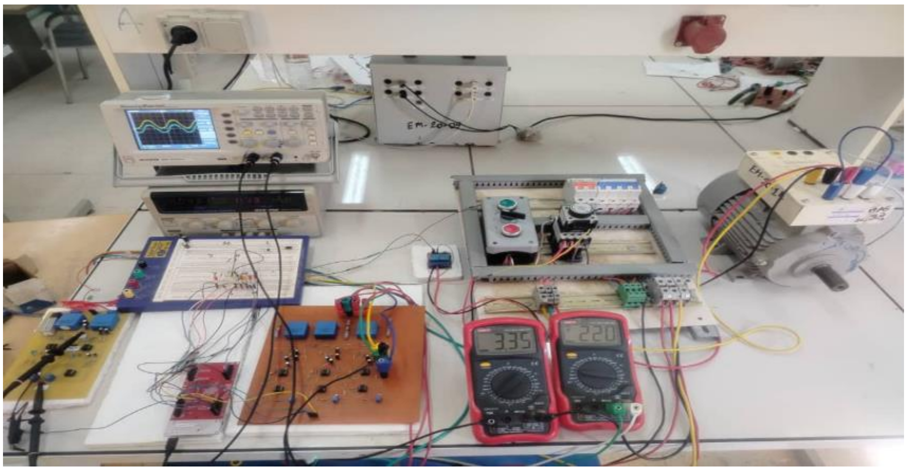

Figure 3.18 : The Global System Setup

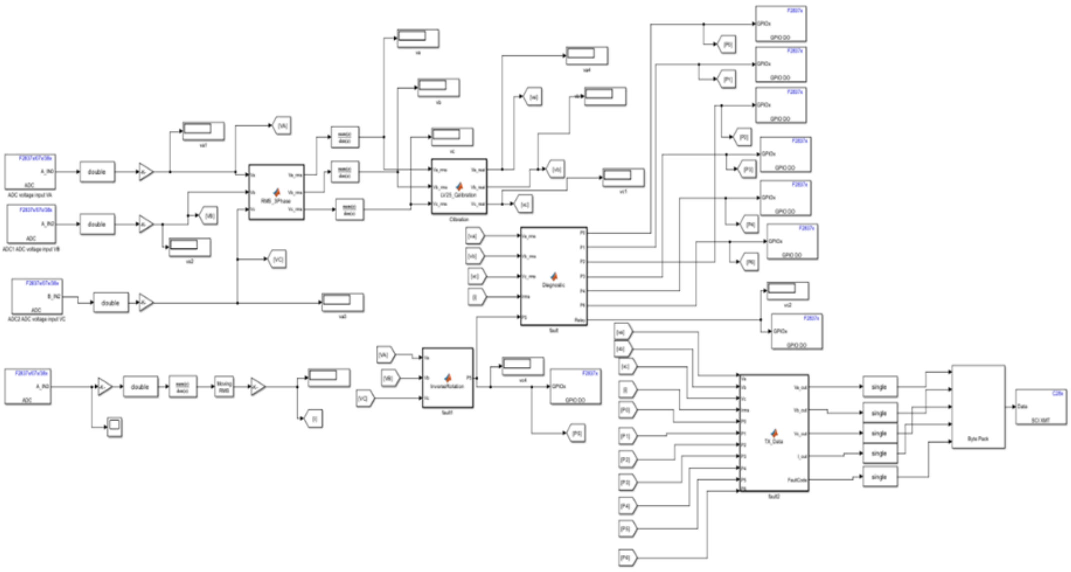

Figure 3.19 : The Global SOFTWARE of the system

3.4.2.1 The Over-Voltage Detection

Overvoltage is detected as soon as one of the three voltages exceeds the threshold of 242 V, which corresponds to 10% of the nominal voltage.

The figure below show the healthy state of the system:

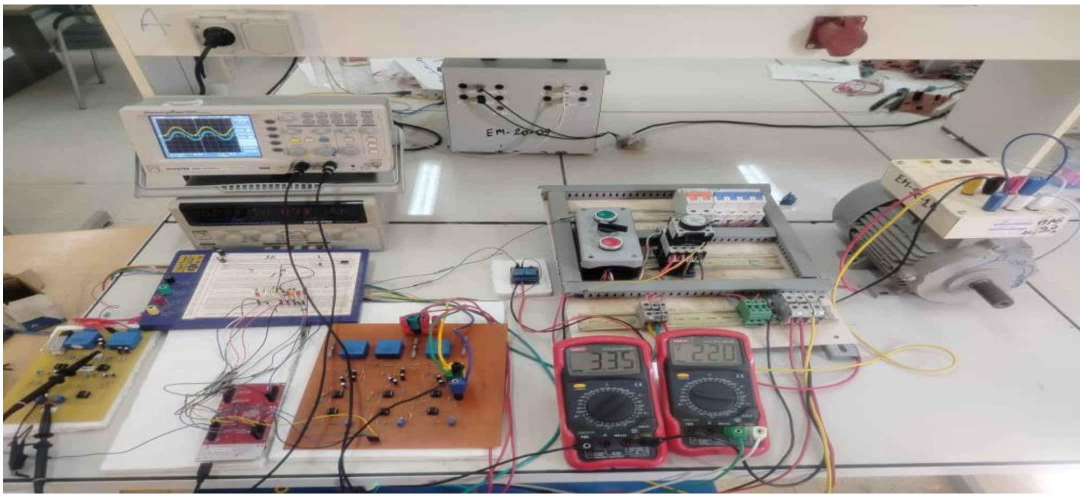

Figure 3.20 : The Healthy state of the System

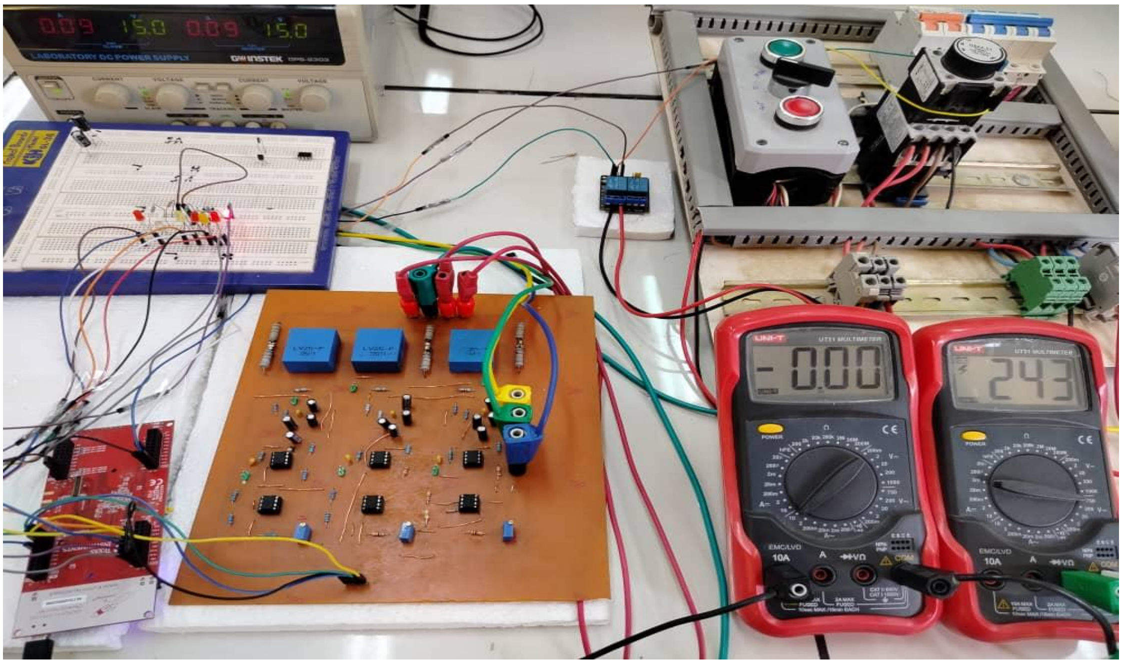

Figure 3.21 : The Over-Voltage state of the System

We observe that the measured voltage exceeds 242 V, which triggers the fault relay. Consequently, the first LED on the right illuminates. This LED specifically corresponds to GPIO 0.

3.4.2.2 The Under-Voltage Detection

Under-voltage is detected as soon as one of the three voltages falls below the threshold of 209 V, which corresponds to 5% of the nominal voltage.

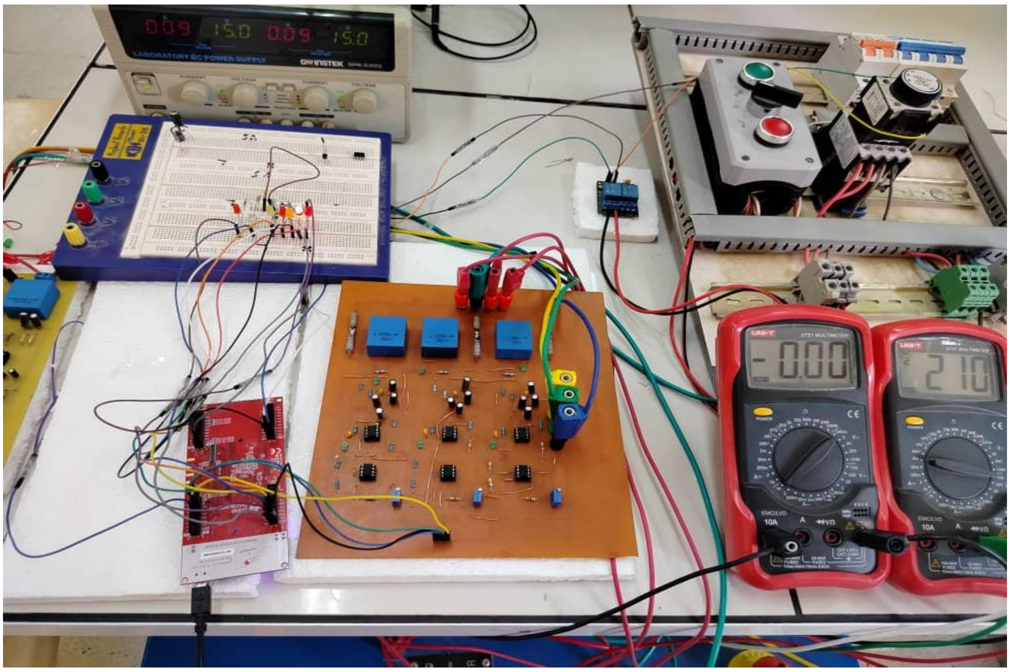

Figure 3.22 : The Under-Voltage state of the System

We observe that the measured voltage falls below 209 V, which triggers the fault relay. Consequently, the 2nd LED on the right illuminates.This LED specifically corresponds to GPIO1.

3.4.2.3 The Over-Load Detection

Over-Load is detected as soon as one of the three Current exceeds the threshold of 4.25 A, which corresponds to 1.25% of the nominal Current.

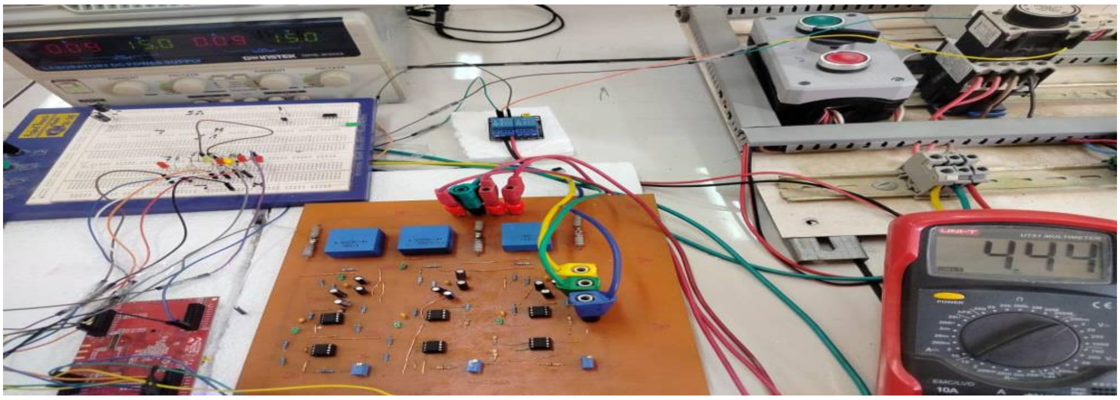

Figure 3.23: The Over-Load state of the System

We observe that the measured current exceeds 4.2 A, which triggers the fault relay. Consequently, the 3rd LED on the right illuminates. This LED specifically corresponds to GPIO 2.

3.4.2.4 The Phase Loss Detection

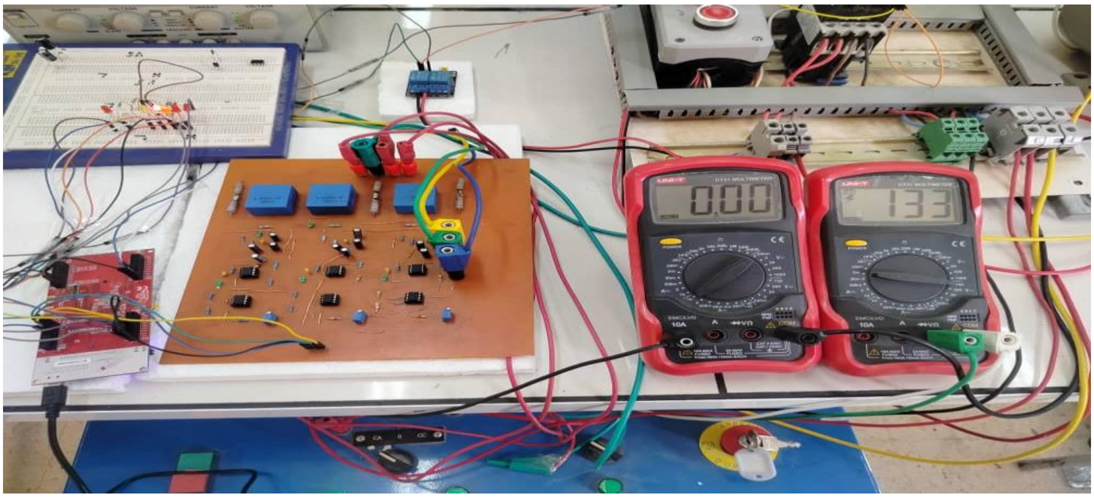

Figure 3.24 : The Phase Loss state of the System

Phase loss is detected as soon as one of the three voltage falls below the threshold of 132 V, which corresponds to 60% of the nominal voltage

We observe that the measured current exceeds 4.2 A, which triggers the fault relay. Consequently, the 4th LED on the right illuminates. This LED specifically corresponds to GPIO 3.

3.4.2.5 The Phase Reversal

Phase inversion is detected from the Clarke transformation, when two phases are reversed.

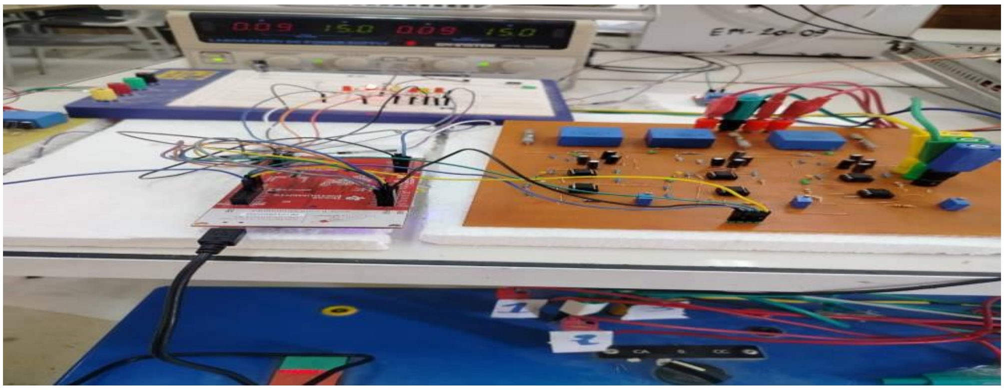

Figure 3.25 : The Phase Reversal state of the System

We have reversed phases 1 and 2, which allows the system to detect the phase reversal. the 5th LED on the right illuminates. This LED specifically corresponds to GPIO4.

3.4.2.6 The Unbalance

To detect the Unbalance, we added a resistor to one of the phases.

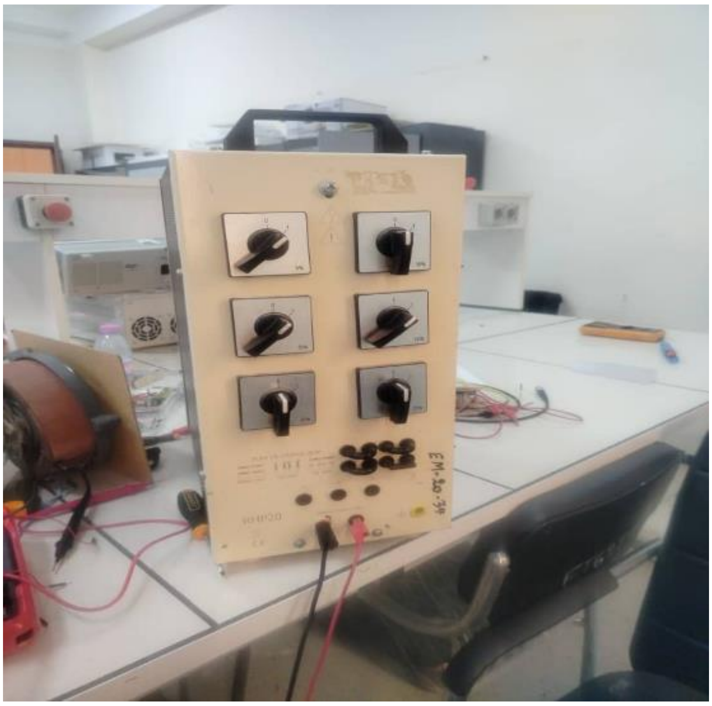

Figure 3.26 : Variable Resistance

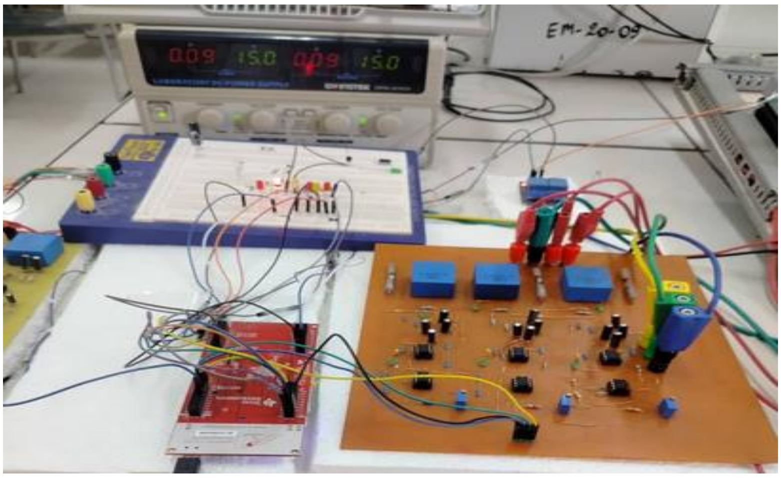

Figure 3.27 : The Unbalance State of the Systeme

The 6th LED on the right illuminates. This LED specifically corresponds to GPIO5

3.4.2.7 The Dry Running Detection

When the operating current drops to between 60% and 80% of the rated current, dry running is detected. In our case, the 80% threshold corresponds to 2.72 A.

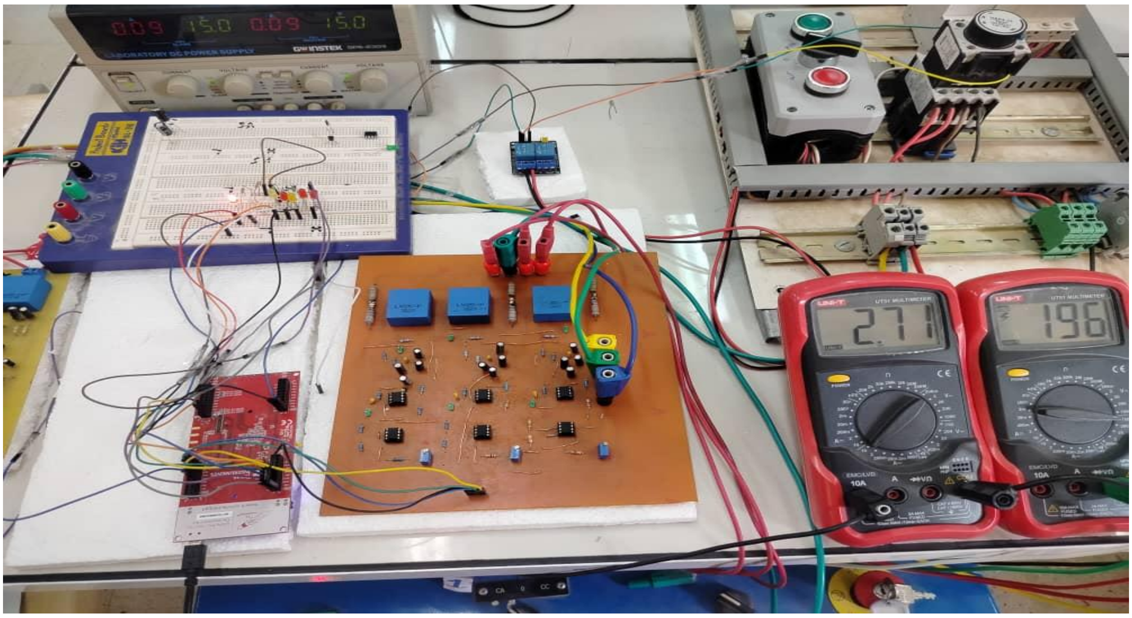

Figure 3.28: The Dry Running State of the Systeme

We observe that the measured current falls below 2.72 A, which triggers the fault relay. Consequently, the 7rd LED on the right illuminates. This LED specifically corresponds to GPIO 6.

3.4.3 The implementation of the IoT monitoring system

The proposed system is based on an IoT architecture in which the TMS320F28379D serves as the primary control unit. It is connected to a first ESP32 module via UART communication to ensure the acquisition and exchange of measurement data.

This first ESP32 is then connected, via LoRa technology, to a second ESP32 located in the field (farmer node), enabling long-distance wireless transmission.

Finally, the second ESP32 is connected to the Wi-Fi network to communicate with a mobile application, thus providing real-time monitoring and control of all system parameters.

This architecture ensures continuous monitoring and reliable, efficient remote control.

Figure 3.29: System Communication Diagram

After wiring and configuring the various components of the communication system, the system is functional and we obtained the following results:

Figure 3.30: Examples of application functionality

3.4.3.1 The healthy state of the system :

In the absence of a detected fault and under nominal parameters, the system provides us with the following readings:

Figure 3.31: The 1st ESP32(Node) serial monitor readings(Healthy state).

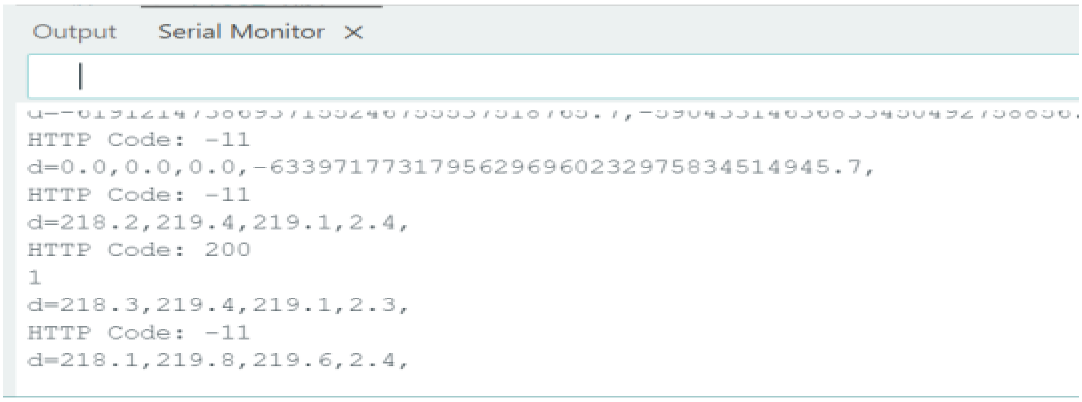

Figure 3.32: The 2nd ESP32(Gateway) serial monitor readings

Figure 3.33: The Mobile APP readings

The C2000 board sends faults to the ESP32 (node) in code form, as follows:

1. Healthy state = code fault 0
2. Over-Voltage = code fault 1
3. Under-Voltage= code fault 2
4. Over-load = code fault 3
5. Phase loss =code fault 4
6. Unbalance = code fault 5
7. Dry running = code fault 6
8. Inverse Rotation = code fault 7

However the ESP32(gateway) decode this fault code into the faults name

3.4.3.2 The Over Voltage detection :

The overvoltage test, carried out by increasing the voltage of one phase up to the overvoltage threshold (242 V), gave us the following results:

```
LoRa Packet Sent
Va=249.59 Vb=248.90 Vc=259.39 I=3.63 Fault=1.00
LoRa Packet Sent
```

Figure 3.34: The 1st ESP32(Node) Over Voltage readings

```
d=250.2,248.5,259.2,3.6,OV
d=250.2,248.6,259.2,3.6,OV
d=250.2,248.7,259.2,3.7,OV
d=250.2,248.7,259.2,3.7,OV
d=0.0,0.0,-3268.2,-0.0,
```

Figure 3.35: The 2nd ESP32(Gateway) Over Voltage readings

3.4.3.3 The Under Voltage detection :

The Under voltage test, carried out by decreasing the voltage of one phase up to the under voltage threshold (209 V), gave us the following results:

```
LoRa Packet Sent
Va=194.14 Vb=196.94 Vc=194.38 I=2.03 Fault=2.00
LoRa Packet Sent
Va=194.14 Vb=196.94 Vc=194.36 I=2.04 Fault=2.00
LoRa Packet Sent
```

Figure 3.36: The 1st ESP32(Node) Under Voltage readings

```
d=194.2,197.0,194.5,1.9,UV
d=0.0,0.0,-19046402097706341294269
d=194.2,197.0,194.5,1.9,UV
d=0.0,0.0,-15708019522818592150770
d=194.2,197.0,194.5,2.0,UV
d=-57633379582992789735840.2,-0.0,
d=194.2,197.0,194.5,2.0,UV
```

Figure 3.37: The 2nd ESP32(Gateway) Under Voltage readings

3.4.3.4 The OverLoad detection:

The Overload test, carried out by increasing the current above threshold (1.25*nominal A), gave us the following results:

```
LoRa Packet Sent
Va=236.38 Vb=236.44 Vc=239.47 I=2.95 Fault=3.00
LoRa Packet Sent
```

Figure 3.38: The 1st ESP32(Node) Over load readings

```
d=236.6,236.2,239.3,2.9,OL
d=236.6,236.2,239.2,2.9,OL
d=236.7,236.2,239.1,2.9,OL
d=236.8,236.2,239.1,2.9,OL
```

Figure 3.39: The 2nd ESP32(Gateway) Over load readings

3.4.3.5 The Phase loss detection:

The phase loss, carried out by decreasing the voltage of one phase unders threshold (132V), gave us the following results:

```
LoRa Packet Sent
Va=126.65 Vb=124.95 Vc=124.90 I=0.50 Fault=4.00
LoRa Packet Sent
Va=126.61 Vb=124.89 Vc=124.87 I=0.59 Fault=4.00
LoRa Packet Sent
Va=126.57 Vb=124.84 Vc=124.84 I=0.58 Fault=4.00
LoRa Packet Sent
```

Figure 3.40: The 1st ESP32(Node) Phase Loss readings

```
d=236.6,236.2,239.3,2.9,OL
d=236.6,236.2,239.2,2.9,OL
d=236.7,236.2,239.1,2.9,OL
d=236.8,236.2,239.1,2.9,OL
```

Figure 3.41: The 2nd ESP32(Gateway) Phase loss readings

3.4.3.6 The Dry Running detection:

The Dry running , carried out by decreasing the current under threshold (0.6*nominal A), gave us the following results

```
LoRa Packet Sent
Va=209.29 Vb=210.81 Vc=210.57 I=2.11 Fault=6.00
LoRa Packet Sent
Va=209.31 Vb=210.78 Vc=210.60 I=2.15 Fault=6.00
LoRa Packet Sent
```

Figure 3.42: The 1st ESP32(Node) Dry Running readings

```
d=208.6,210.5,210.4,2.3,
HTTP Code: -1
d=0.0,0.0,0.0,0.0,
HTTP Code: -1
d=208.8,210.5,210.5,2.1,DRY RUNNING
HTTP Code: -1
d=208.6,210.9,210.5,2.1,DRY RUNNING
HTTP Code: -1
```

Figure 3.43: The 2nd ESP32(Gateway) Dry Running readings

3.4.3.7 The Inverse Rotation detection:

The inverse rotation , carried out by inversing any two phases gave us the following results:

```
LoRa Packet Sent
Va=219.78 Vb=219.33 Vc=221.10 I=2.46 Fault=7.00
LoRa Packet Sent
Va=219.82 Vb=219.35 Vc=221.08 I=2.48 Fault=7.00
LoRa Packet Sent
Va=219.84 Vb=219.36 Vc=221.08 I=2.45 Fault=7.00
LoRa Packet Sent
Va=219.86 Vb=219.39 Vc=221.10 I=2.47 Fault=7.00
```

Figure 3.44: The 1st ESP32(Node) Inverse Rotation readings

```
d=-0.0,0.0,0.0,-0.0,
HTTP Code: 200
1
d=219.8,219.6,219.4,2.5,INVERSE ROTATION
HTTP Code: 200
1
d=219.9,219.6,219.5,2.5,INVERSE ROTATION
HTTP Code: 200
```

Figure 3.45: The 2nd ESP32(Gateway) Inverse Rotation readings

3.4.3.8 Examples of the mobile APP readings:

The systeme give us a continus readings of : Voltages, current and the systeme state. if any fault is detected a notiffication is send into the mobile App in real-time

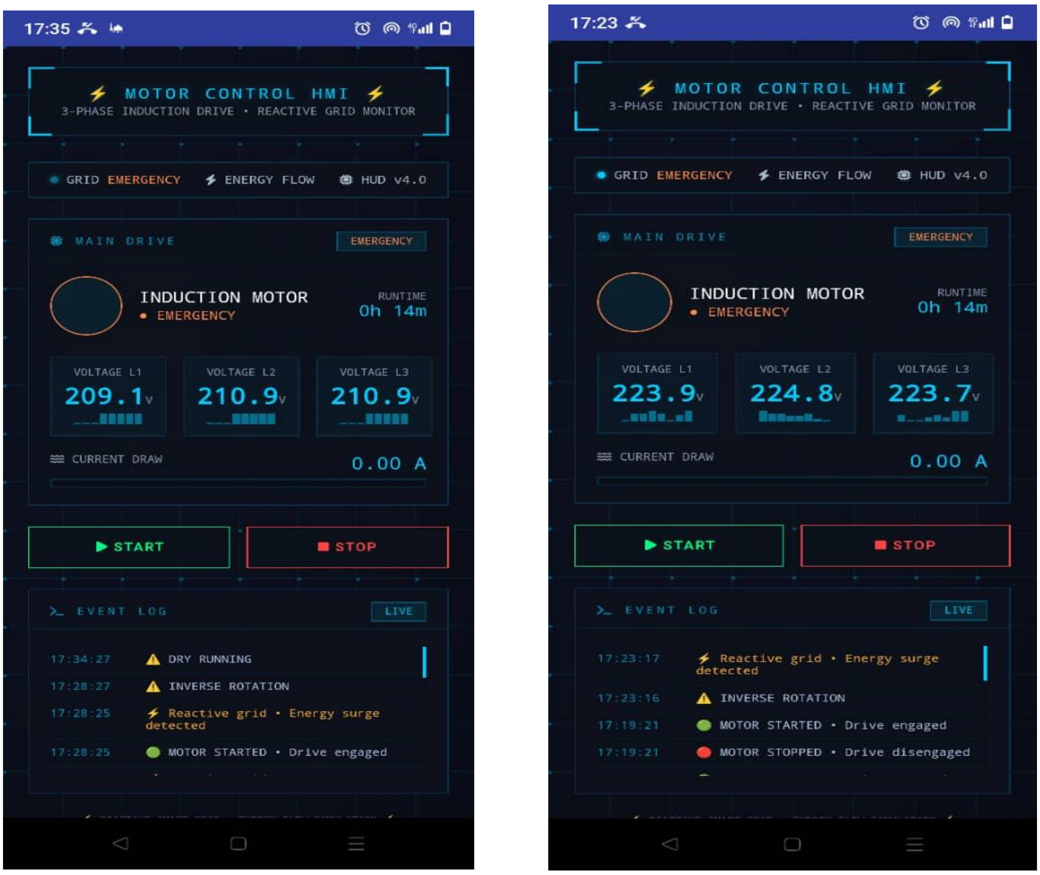

Figure 3.46: examples of fault notifications in the Mobile APP

After various trials and tests carried out on the system, it has demonstrated high efficiency in detecting faults and making appropriate decisions in real time, including stopping the engine to avoid greater damage that could result from continued operation. The precise measurement of current and voltage values through the analog-to-digital converters (ADCs) of the TMS320 C2000 board, using the LV25-P and LA25-NP sensors, alone constitutes a significant contribution to the performance of the system.

Thanks to its advanced technical characteristics, notably a clock frequency of 200 MHz and a RAM memory of 204 KB, the C2000 card represents a central processing unit particularly suited to this application. It ensures the reading, processing and transmission of data in real time with great reliability. In addition, it allows the use of the UART protocol to communicate with the ESP32 Node, which acts as an interface between the TMS320 main unit and the user.

This communication is carried out via the ESP32 Gateway using LoRa technology, which allows data transmission without depending on cellular network coverage or a Wi-Fi connection. The ESP32 Gateway then liaises with the server and the mobile application to instantly transmit current and voltage values as well as information relating to detected faults.

All of these technological choices give the system great efficiency, excellent flexibility and strong adaptability, allowing its use both in urban environments and in remote areas or areas lacking conventional communication infrastructure. Furthermore, the mobile application developed as part of this project stands out for its user-friendly and intuitive interface, facilitating its installation and handling by users. It allows rapid consultation of real-time data as well as simple access to information relating to the state of the system and detected faults, thus helping to improve the user experience and the effectiveness of supervision.

3.5 Conclusion

In conclusion, this chapter has provided a detailed presentation of the implementation and experimental validation phase of the developed system. Tests conducted under real-world conditions first confirmed the proper functioning of the voltage and current signal conditioning boards, particularly regarding signal filtering, shifting, and adaptation to ensure compatibility with the ADC inputs of the TMS320F28379D microcontroller.

Subsequently, the various fault scenarios studied (overvoltage, undervoltage, phase imbalance, phase inversion, and no-load operation) were implemented and tested. The results obtained demonstrate that the system provides reliable and rapid detection of these anomalies, as well as accurate signaling via the GPIO outputs and LED indicators.

In parallel, the implemented IoT architecture, based on the ESP32, has proven its effectiveness. Communication between the TMS320F28379D and the ESP32 via UART enabled the real-time acquisition of electrical measurements. This data is then transmitted to a second ESP32 via LoRa technology, ensuring long-range wireless communication. This second ESP32 is connected to the Wi-Fi network to transmit the data to the server and display it on the mobile application.

The mobile application plays a central role in the system, allowing the user to monitor the motor's electrical parameters in real time, view fault status, and send control commands (START/STOP). Thus, the entire system guarantees continuous monitoring, reliable remote control, and real-time data visualization.

Finally, the results obtained confirm the robustness, accuracy, and reliability of the proposed architecture, thereby validating the overall effectiveness of the developed IoT system.

Generale conclusion

The system we designed represents the result of comprehensive and rigorous work, from hardware design to software implementation. Indeed, we developed the entire architecture, from PCB design to the creation of the mobile application enabling remote control and monitoring of the irrigation system.

Significant work was carried out on the TMS320F28379D microcontroller, particularly for the calibration of voltage and current measurements. This step alone constitutes a complex and relatively unexplored area of study, due to the difficulty of implementation and the limited number of similar works in the literature.

Furthermore, we ensured communication between the TMS320F28379D and the ESP32 modules via UART, as well as communication between two ESP32 boards using LoRa technology, which allows for reliable data transmission even in remote areas without Wi-Fi or GSM network coverage.

Moreover, the integration of a web server connected to the mobile application has enabled real-time monitoring and simple, effective remote control. The addition of an intelligent fault detection system has also made it possible to replace traditional protection devices, thus offering a more modern, reliable solution better suited to the requirements of current irrigation systems.

Therefore, the developed system provides an effective response to the problems faced by farmers, including financial losses, management difficulties, and time constraints. It allows for simplified remote control, improved monitoring of system parameters, and ensures smooth irrigation operations under optimal conditions, even in isolated areas.

Finally, this work can be improved and expanded by integrating advanced artificial intelligence techniques such as fuzzy logic or deep learning, as well as adding new sensors (temperature, humidity, vibration, etc.). These future improvements will further enhance the system's performance, flexibility, and autonomy in the face of varying environmental conditions.

List of References

[1] Vallejo-Gómez D, Osorio M, Hincapié CA. Smart Irrigation Systems in Agriculture: A Systematic Review. Agronomy. 2023 ; 13(2) :342.

[2] Jaiswal N, Kumar TV, Shukla C. Smart drip irrigation systems using IoT: a review of architectures, machine learning models, and emerging trends. Discover Agriculture. 2025 ; 3:253.

[3] Dutta S, Gorain S, Roy S, Banerjee S, Sah RP. Integrating IoT and communication technologies for smart and precision irrigation systems toward sustainable water management. Discover Internet of Things. 2026.

[4] Elhoseny M, et al. Recent advances in IoT-driven crop monitoring and precision irrigation: Technologies, models, and future challenges. Smart Agricultural Technology. 2026.

[5] Pérez-Castro N, et al. Data-driven water need estimation for IoT-based smart irrigation: A survey. Expert Systems with Applications. 2023; 225: 120194.

[6] The application of machine learning techniques for smart irrigation systems: A systematic literature review. Smart Agricultural Technology. 2024; 7: 100425.

[7] Taueatsoala K, Daniels C, Ramsunar AJ, Bronkhorst P, Ezugwu AE. TinyML-Enabled IoT for Sustainable Precision Irrigation. ArXiv. 2026.

[8] Neduncheliyan S, Kazuaki T, Krishnamoorthy R, Thiagarajan R, Swarna B, Kumar A. Comparative analysis of machine learning and novel deep learning models for IoT enabled smart irrigation water management system. Discover Internet of Things. 2026.

[9] Bandyopadhyay D, Sen J. Internet of Things: Applications and Challenges in Technology and Standardization. Wirel Pers Commun. 2011;58(1):49–69.

[10] Islam MM, Nooruddin S, Karray F, Muhammad G. Internet of Things Device Capabilities, Architectures, Protocols, and Smart Applications in Healthcare Domain: A Review. IEEE Access. 2022 ; 10:23946–80.

[11] Li L, Zhang Q. State-of-the-Art Internet of Things in Protected Agriculture. Sensors. 2019 ; 19(8) :1833.

[12] Pereira GP, Chaari MZ, Daroge F. IoT-Enabled Smart Drip Irrigation System Using ESP32. IoT. 2023 ; 4(3) :221–243.

[13] IoT-enabled smart agriculture for improving water management: A smart irrigation control using embedded systems and Server-Sent Events. Scientific African. 2025 ; 27.

[14] Boukri Y, Hamici HS, Mansour RF, Maamar AET, Ghoneim SSM, Paramasivam P, et al. Analysis and experimental implementation of affordable smart irrigation system using IoT to reduce agricultural costs and minimize water usage. Applied Water Science. 2026;16:36.

[15] IoT Based Smart Agriculture Monitoring and Irrigation System Using Renewable Energy. Int J Progressive Research in Science and Engineering. 2024.

[16] IoT System with ESP32 for Smart Drip Irrigation and Climate Monitoring in Greenhouses. Emerging Science Journal. 2025.

[17] Internet of Things (IoT)-Based Smart Agriculture Irrigation and Monitoring System Using Ubidots Server. Engineering Proceedings. 2024.

[18] Fuzzy-Adaptive Smart Irrigation Based on IoT. INSANtek. 2025.

[19] ESP32-Based Smart Irrigation System with Blynk IoT Integration. IJERT. 2026.

[20] Kunt YE. Development of a Smart Autonomous Irrigation System Using IoT and AI. ArXiv. 2025.

[21] Chapman SJ. Electric Machinery Fundamentals. 5th ed. New York : McGraw-Hill Education ; 2011.

[22] IEEE Standards Association. IEEE Std 242-2001: IEEE Recommended Practice for Protection and Coordination of Industrial and Commercial Power Systems. New York: IEEE; 2001.

[23] Fitzgerald AE, Kingsley C, Umans SD. Electric Machinery. 7th Ed. New York: McGraw-Hill; 2013.

[24] Pillay P, Manyage M. Definitions of voltage unbalance. IEEE Power Engineering Review. 2001;21(5):50–51.

[25] Karassik IJ, Messina JP, Cooper P, Heald CC. Pump Handbook. 4th ed. New York : McGraw-Hill ; 2008.

[26] Bhatia A. Motor Protection Principles 101. Continuing Education and Development Inc. (CED Engineering); 2012.

[27] International Electrotechnical Commission. IEC 60034-1: Rotating Electrical Machines – Part 1: Rating and Performance. Geneva: IEC ; 2022.

[28] IEEE Standards Association. IEEE Std 141-1993: IEEE Recommended Practice for Electric Power Distribution for Industrial Plants. New York : IEEE ; 1994.

[29] TestGuy. PQ Analysis: Undervoltage, Overvoltage, Sags, Swells [Internet]. 2019 Nov 23 [cited 2026 Jun 4]. Available from: https://testguy.net/content/266-PQ-Analysis-Undervoltage-Overvoltage-Sags-Swells

[30] Bhatia A. Motor Protection Principles 101. Continuing Education and Development Inc. (CED Engineering); 2012.

[31] National Electrical Manufacturers Association. NEMA MG 1: Motors and Generators. Rosslyn (VA): NEMA; 2024.

[32] International Electrotechnical Commission. IEC 60034-26: Effects of Unbalanced Voltages on Three-Phase Cage Induction Motors. Geneva: IEC; 2026.

[33] Bishop T. Correcting unbalanced voltage situations. EC&M Magazine. 2014.

[34] Electrical Engineering Portal. The influence of voltage unbalance on NEMA motor performance. 2016.

[35] Shah K. What is voltage unbalance? [Internet]. Engineers Hub. 2023 Jun 17 [cited 2026 Jun 4]. Available from: https://engineershub.co.in/what-is-voltage-unbalance/

[36] International Electrotechnical Commission. IEC 60034-1:2026: Rotating electrical machines – Part 1: Rating and performance. 15th ed. Geneva : IEC ; 2026.

[37] International Electrotechnical Commission. IEC 60947-4-1:2023: Low-voltage switchgear and controlgear – Part 4-1: Contactors and motor-starters – Electromechanical contactors and motor-starters. 5th ed. Geneva : IEC ; 2023.

[38] International Electrotechnical Commission. IEC 60034-11:2020: Rotating electrical machines – Part 11: Thermal protection. Geneva: IEC; 2020.

[39] ABB. Tripping classes of thermal overload relays according to IEC 60947-4-1. Zurich:

[40] Otomasyon AVM. What is OC (Overcurrent) fault? [Internet]. Otomasyon AVM; 2025 [cited 2026 Jun 5]. Available from: Otomasyon AVM - What is OC (Overcurrent) faultABB; n.d.

[41] Schneider Electric. Phase sequence and phase failure protection in three-phase systems [Internet]. Rueil-Malmaison: Schneider Electric; 2024 [cited 2026 Jun 5].60 be 41

[42] IEEE Industry Applications Society. Protective relaying and phase sequence monitoring for three-phase systems. IEEE Trans Ind Appl. 2019;55(4):3921–3929.

[43] International Electrotechnical Commission. IEC 60204-1: Safety of machinery – Electrical equipment of machines – Part 1: General requirements. Geneva : IEC ; 2016.

[44] WEG Electric Corp. Dry run protection for centrifugal pumps [Internet]. Duluth : WEG ; 2023 [cited 2026 Jun 5].

[45] ABB. Motor protection and control handbook. Zurich: ABB Group; 2021.

[46] LEM International SA. LEM: Global leader in electrical measurement solutions [Internet]. Meyrin (Switzerland): LEM International SA; 2026 [cited 2026 Jun 6]. www.lem.com

[47] Espressif Systems. ESP32-WROOM-32 Datasheet [Internet]. Shanghai: Espressif Systems;2024[citéle6juin2026].https://www.espressif.com/en/products/socs/esp32/documentation.

[48] Semtech Corporation. SX1276/77/78/79 – LoRa Modem Designer's Guide and Datasheet [Internet]. Camarillo (CA): Semtech Corporation; 2024 [cité le 6 juin 2026]. Disponible sur: https://www.semtech.com/products/wireless-rf/lora-connect/sx1278

[49] Texas Instruments. *TMS320F2837xD Dual-Core Microcontrollers Datasheet (TMS320F28379D)* [Internet]. Dallas (TX): Texas Instruments; 2024 [cited 2026 Jun 12]. Available from: https://www.ti.com/lit/ds/symlink/tms320f28379d.pdf